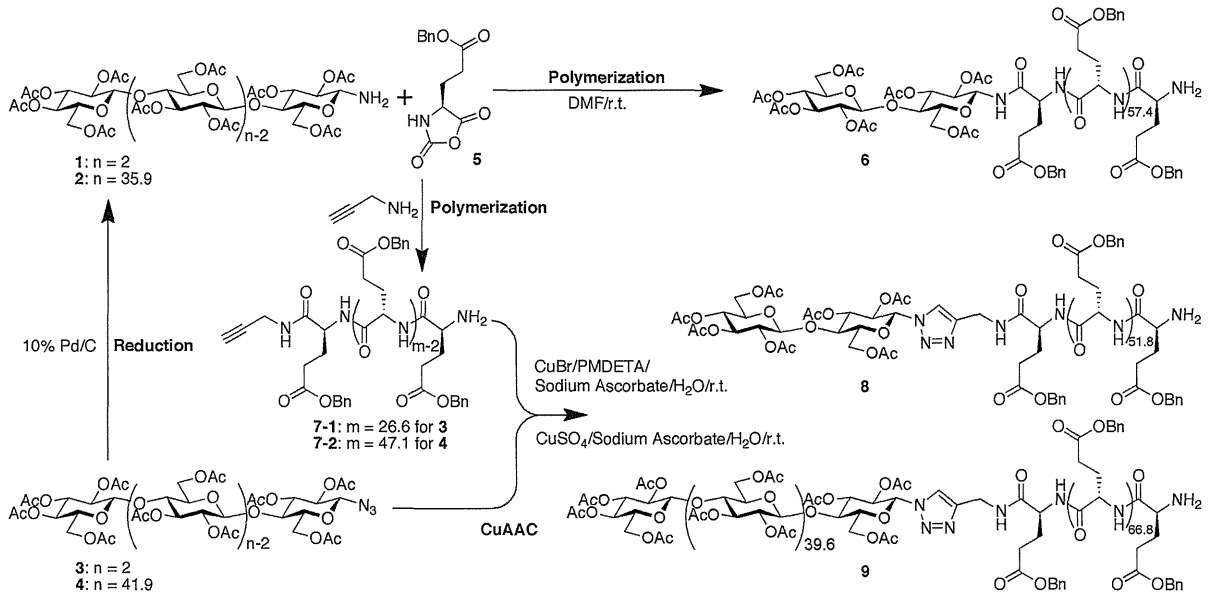

Scheme 1 Synthesis routes for C2TA-*b*-PBLG (**6**) via ring-opening polymerization of BLG NCA (**5**) initiated from amino-functionalized cellulose derivatives (**1**) and for C2TA-*b*-PBLG (**8**) and CTA-*b*-PBLG (**9**) via CuAAC between azido-functionalized C2TA-N_3 (**3**) or CTA-N_3 (**4**) and alkyne-functionalized PBLG (**7**). (The chemical structures of the N-termini of compounds **7**, **8**, and **9** are not exactly drawn; see "Materials and methods" section.)

DP = 19, $[M + Na]^+$ = 4,355.858; DP = 20, $[M + Na]^+$ = 4,575.410; DP = 21, $[M + Na]^+$ = 4,794.315; DP = 22, $[M + Na]^+$ = 5,013.887; DP = 23, $[M + Na]^+$ = 5,233.070; DP = 24, $[M + Na]^+$ = 5,453.077; carboxyl end group series (Cao et al. 2012), *m/z* DP = 14, $[M + H]^+$ = 3,388.627; DP = 15, $[M + H]^+$ = 3,608.965; DP = 16, $[M + H]^+$ = 3,827.815; DP = 17, $[M + H]^+$ = 4,047.109; DP = 18, $[M + H]^+$ = 4,266.354; DP = 19, $[M + H]^+$ = 4,485.536; DP = 20, $[M + H]^+$ = 4,703.741; DP = 21, $[M + H]^+$ = 4,923.701; DP = 22, $[M + H]^+$ = 5,143.429; DP = 23, $[M + H]^+$ = 5,362.840, 500 MHz ^{1}H-NMR ($CDCl_3$): δ 2.27 (Hβ), 2.60 (Hγ), 3.94 (Hα), 5.04 (OCH_2Ph), 7.2–7-4 (aromatic H); 125 MHz ^{13}C-NMR ($CDCl_3$): δ 25.5 (Cβ), 30.9 (Cγ), 56.8 (Cα), 66.1 (OCH_2Ph), 128.1, 128.5, 136.0 (aromatic C), 172.0 (Cδ=O), 175.3 (CαC=O); DSC: T_g = approx. 10 °C; T_{dec} = over 270 °C.

Synthesis of 2,3,4,6-tetra-*O*-acetyl-β-D-glucopyranosyl-(1 → 4)- 2,3,6-tri-*O*-acetyl-β-D-glucopyranosylazide-*block*-poly(γ-benzyl-L-glutamate) (8)

To a solution of 2,3,4,6-tetra-*O*-acetyl-β-D-glucopyranosyl-(1 → 4)-2,3,6-tri-*O*-acetyl-β-D-glucopyranosylazide (**3**, C2TA-N_3) (3.8 mg) and alkyne-functionalized poly(γ-benzyl-L-glutamate) (**7-1**, 22.6 mg, DP_n = 26.6) in anhydrous DMF (1.0 mL), *N,N,N′,N″,N‴*-pentamethyldiethylenetriamine (PMDETA) (16.0 μL), and an aqueous solution of sodium ascorbate (30.3 mg/38 μL) were added. The reaction mixture was degassed. Copper(I) bromide (11.0 mg) was then added to the reaction mixture. The reaction mixture was stirred under nitrogen atmosphere at r.t. for 27 h. The reaction product was concentrated to dryness. The crude product was washed with distilled water, and methanol to afford diblock copolymer **8** (19.7 mg, 78 % yield). MALDI-TOF MS analysis revealed that all the PBLG blocks feature pyroglutamate (Habraken et al. 2011) end groups. MALDI-TOF MS (positive linear mode, DHB used as a matrix) *m/z* DP = 6, $[M + Na]^+$ = 1,946.418; DP = 7, $[M + Na]^+$ = 2,165.414; DP = 8, $[M + Na]^+$ = 2,384.429; DP = 9, $[M + Na]^+$ = 2,603.416; DP = 10, $[M + Na]^+$ = 2,822.470; DP = 11, $[M + Na]^+$ = 3,041.134; DP = 12, $[M + Na]^+$ = 3,260.851; DP = 13, $[M + Na]^+$ = 3,480.163; DP = 14, $[M + Na]^+$ = 3,699.231; DP = 15, $[M + Na]^+$ = 3,918.447; DP = 16, $[M + Na]^+$ = 4,137.948; DP = 17, $[M + Na]^+$ = 4,356.637; DP = 18, $[M + Na]^+$ = 4,574.933; DP = 19, $[M + Na]^+$ = 4,795.813; DP = 20, $[M + Na]^+$ = 5,013.299;

Table 1 Synthesis of C2TA-*b*-PBLG (**6**) via ROP of BLG NCA (**5**)

Initiator	Comp. no.	Molecular weight				Diblock copolymer								
						Comp. no.	(Initiator)/(amino acid NCA)		Molecular weight					
		M_n	10^{-3} M_n	10^{-3} M_w	DP_n			Yield (%)	10^{-3} M_n	10^{-3} M_w	M_w/M_n	$DP_{n,\ GPC}$ of PBLG	$DP_{n,\ NMR}$ of PBLG
C2TA-NH_2	**1**	635.57	–	–	2	**6**[a]	1/15	70	2.7	5.2	2.0	9.2	59.4
CTA-NH_2	**2**	–	10	18	35.9	–	1/15	Trace	–	–	–	–	–

[a] Aggregation of diblock copolymers was observed. DP of oligopeptide blocks was estimated by GPC

DP = 21, $[M + Na]^+$ = 5,233.066; DP = 22, $[M + Na]^+$ = 5,452.221; DP = 23, $[M + Na]^+$ = 5,672.760. Number-averaged molecular weight (DP_n) of alkyne-functionalized PBLG calculated by ^{1}H-NMR measured in $CDCl_3$ with 15 % trifluoroacetic acid: 26.6; molecular weight in $CHCl_3$ was estimated by GPC. Number-averaged molecular weight: 1.9×10^3; weight-averaged molecular weight: 2.6×10^3, DP_n calculated by ^{1}H-NMR measured in $CDCl_3$: 53.8. 500 MHz ^{1}H-NMR ($CDCl_3$): δ 1.98–2.09 (CH_3CO), 2.28 (Hβ), 2.59 (Hγ), 3.92 (Hα), 5.03 (OCH_2Ph), 7.2–7.4 (aromatic protons), 8.33 (NH); 125 MHz ^{13}C-NMR ($CDCl_3$): δ 20.5 (CH_3CO), 25.6 (Cβ), 30.9 (Cγ), 56.8 (Cα), 66.2 (OCH_2Ph), 128.1, 128.5, 136.0 (aromatic C), 172.0 (Cδ=O), 175.4 (CαC=O). Note that the carbon resonances of the cellobiosyl residue were hidden in the baseline noise.

Synthesis of tri-*O*-acetyl cellulose-*block*-poly(γ-benzyl-L-glutamate) (9)

To a solution of tri-*O*-acetyl cellulosylazide (**4**, 50.1 mg, DP_n = 41.6) and alkyne-functionalized poly(γ-benzyl-L-glutamate) (**7-2**, 134.0 mg, DP_n = 47.1) in DMSO (3 mL), an aqueous solution of copper(II) sulfate pentahydrate (12 mg/50 μL) and an aqueous solution of sodium ascorbate (20.5 mg/50 μL) were added. The reaction mixture was stirred at r.t. for 21 h. The reaction mixture was added into a large excess of methanol, and the precipitate was collected by centrifugation (15,000 rpm, 10 min) to afford crude tri-*O*-acetyl cellulose-*block*-poly(γ-benzyl-L-glutamate) (159.2 mg). The crude CTA-*b*-PBLG was purified by gel filtration chromatography (LH-60, eluent: methanol/dichloromethane 1/4, v/v) to afford pure diblock copolymer CTA-*b*-PBLG (**9**) (84.3 mg, 85 % yield). Number-averaged degree of polymerization (DP_n) of the PBLG segment calculated by ^{1}H-NMR measured in $CDCl_3$: 68.8, based on the supposition that DP_n of the CTA segment is 41.6; molecular weight estimated by GPC: number-averaged molecular weight of **9**: 2.7×10^3; weight-averaged molecular weight of **9**: 9.5×10^3, 500 MHz ^{1}H-NMR ($CDCl_3$): δ 1.94, 2.01, 2.13 (CH_3CO), 2.26 (Hβ), 2.59 (Hγ), 3.55 (H5), 3.72 (t, J = 8.5, H4), 3.93 (Hα), 4.07 (d, J = 7.0, H6), 4.38 (d, J = 10.5, H6), 4.42 (d, J = 7.0, H1), 4.80 (t, J = 8.0, H2), 5.0–5.2 (H3 and OCH_2Ph), 7.2–7.4 (aromatic H), 8.01 (H at position 5 of 1,4-disubstituted 1,2,3-triazole); 125 MHz ^{13}C-NMR ($CDCl_3$): δ 20.4, 20.5, 20.8 (CH_3CO), 25.5 (Cβ), 30.8 (Cγ), 56.8 (Cα), 62.0 (C6), 66.1 (OCH_2Ph), 71.8 (C2), 72.5 (C3), 72.8 (C5), 76.0 (C4), 100.5 (C1), 128.1, 128.4, 136.0 (aromatic C), 169.3, 169.7, 170.2 (CH_3CO), 172.0 (Cδ=O), 175.4 (CαC=O); DSC: T_g of PBLG segment = approx. 10 °C; T_g of CTA segment = approx. 144 °C; T_c of CTA segment = 205 °C.

Atomic force microscopy (AFM), field emission scanning electron microscopy (FE-SEM) and transmission electron microscopy (TEM)

A few drops of a 0.1 wt% solution of CTA-*b*-PBLG (**9**) in dichloromethane were dropped, spin-coated at 1,000 rpm for 30 s, and dried on the surface of a silicon wafer. The obtained thin film of CTA-*b*-PBLG was dried under vacuum at r.t. for 6 days, and observed under an atomic force microscopy (SPM-9600, Shimadzu) in dynamic and phase modes. The thin film of CTA-*b*-PBLG was then annealed under vacuum at 180 °C for 24 h, and observed under an AFM in dynamic and phase modes. The cantilever probe (Olympus, OMCL-AC240TS-C2 or OMCL-AC200TS-C3) was used.

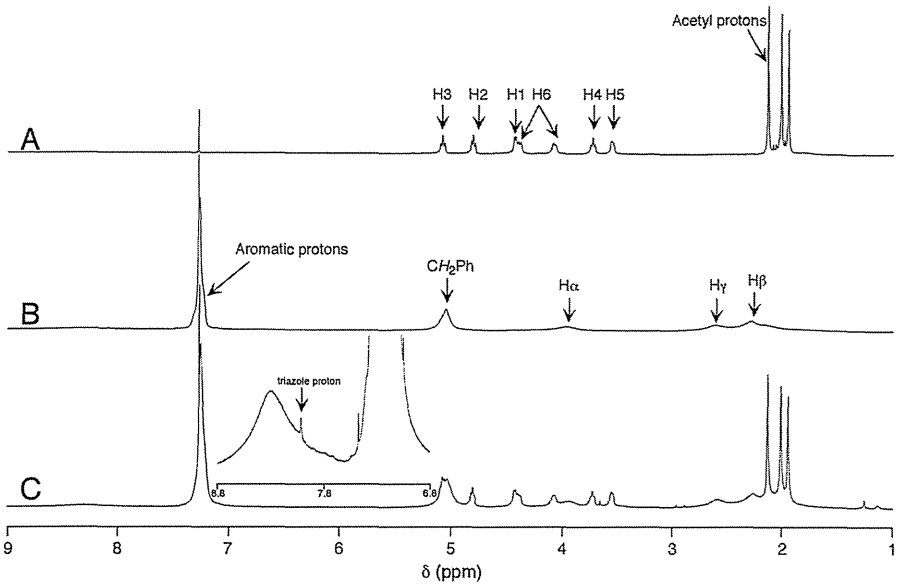

Fig. 1 ^{1}H NMR spectra of **A** azido-functionalized cellulose triacetate (**4**), **B** alkyne-functionalized PBLG (**7-2**), and **C** CTA-*b*-PBLG (**9**)

A few drops of a 0.1 wt% solution of CTA-*b*-PBLG (**9**) in chloroform were dropped and dried on the surface of a silicon wafer. The obtained thin film of CTA-*b*-PBLG was annealed at 180 °C for 24 h and stained overnight by the vapor of a 0.5 % aq. RuO_4 solution at room temperature. The surface of the film was observed under a field emission scanning electron microscope (S-4800; Hitachi) at an accelerating voltage of 1.5 kV and a 2.5 mm working distance. To visualize the distribution of ruthenium, a back-scattered electron microscopy (BSE) signal was obtained. For better comparison with the TEM images, the BSE signal was inverted.

A block of CTA-*b*-PBLG (**9**) was annealed at 180 °C for 24 h, stained by the vapor of a 0.5 % aq. RuO_4 solution for 24 h at room temperature, and then embedded in epoxy resin. Ultrathin sections were obtained from the epoxy resin-embedded blocks using an ultramicrotome equipped with a diamond knife. The sections were mounted on copper grids with an elastic carbon supporting film (Oken Shoji, Japan) and observed under a transmission electron microscope (JEM1400; JEOL) at an accelerating voltage of 100 kV. It is known that ruthenium tetroxide readily stains many polymers (Trent et al. 1983) and compounds containing double bonds (Howell and Reneker 1990). It is likely that the PBLG block is stained more readily than the CTA block (de Oliveira and Glasser 1994).

Results and discussion

Two strategies

We explored two methods of preparing cellulosic diblock copolymers, as shown in Scheme 1. Anionic ring-opening polymerization (ROP) of BLG NCA (**5**) initiated from cellulose triacetate derivatives as macroinitiators would provide CTA-*b*-PBLG. The second strategy involves a coupling reaction, CuAAC, between azido end-functionalized tri-*O*-acetyl-cellulosylazide (**4**) and alkyne end-functionalized PBLG (**7**). We compared the efficiency of those reactions in producing cellulosic diblock copolymers.

Synthesis of C2TA-*b*-PBLG (6) via ROP of BLG NCA (5)

The reactivity of the macroinitiator, CTA-NH_2 (**2**), for the ROP of BLG NCA (**5**) remains unknown. C2TA-NH_2 (**1**) was therefore selected as a model polymeric cellulose derivative for the ROP initiation reaction of BLG NCA (**5**). The reactivities of the amino groups at the ends of CTA-NH_2 (**2**) and C2TA-NH_2 (**1**) were compared.

Table 1 summarizes the results of the ROP of BLG NCA (**5**) to afford cellulosic diblock copolymers. C2TA-NH_2 (**1**) was able to initiate the ROP of BLG NCA (**5**) to afford C2TA-*b*-PBLG (**6**) with a DP_n of

Table 2 Synthesis of C2TA-*b*-PBLG (**8**) and CTA-*b*-PBLG (**9**) via CuAAC

	Cellulosic segment				PBLG (7)						Diblock copolymer								
	Comp. no.	Molecular weight				Comp. no.	Molecular weight					Comp. no.	(Azide)/(alkyne)	Yield		Molecular weight				
		M_n	10^{-3} M_n	10^{-3} M_w	DP_n		10^{-3} M_n	10^{-3} M_w	M_w/M_n	$DP_{n,GPC}$	$DP_{n,NMR}$			Solv.	(%)	10^{-3} M_n	10^{-3} M_w	M_w/M_n	$DP_{n,GPC}$ of PBLG	$DP_{n,NMR}$ of PBLG
C2TA-N_3	**3**	661.57	–	–	2	**7-1**	0.38	0.52	1.4	1.5	26.6	**8**[a]	1/1.5	DMF	78	1.9	2.6	1.3	5.5	53.8
CTA-N_3	**4**	–	12.1	24.1	41.6	**7-2**	2.2	3.4	1.6	9.8	47.1	**9**	1/2.75	DMSO	85	2.7	9.5	3.6	–	68.8[b]

[a] Molecular weight of a molecularly dispersed part in $CHCl_3$ was estimated by GPC

[b] DP_n of PBLG of CTA-b-PBLG was calculated based on the supposition that DPn of CTA is 41.6

PBLG of 59.4, as calculated from a comparison of the proton resonance area of C2TA with that of PBLG in its ^{1}H-NMR spectrum (see Supporting Information, Figure S1). GPC analysis indicated a DP_n of PBLG of 9.2, which is smaller than that calculated by ^{1}H-NMR, likely because C2TA-*b*-PBLG (**6**) aggregates in chloroform and part of polymer, including the PBLG segment, was probably removed when filtering the solution (pore size: 2.7 μm) or by the guard column. The NMR measurement of **6** in $CDCl_3$ afforded a convincing DP_n 59.4. In contrast, CTA-NH_2 (**2**) did not initiate the ROP of BLG NCA (**5**). We concluded that either the amino functional group at the end of tri-*O*-acetyl cellulose is not sufficiently nucleophilic to initiate the ROP of PBLG or the bulkiness of the CTA segment disturbs the ROP initiation process. We therefore investigated a second strategy, using Cu-AAC, to reach the cellulosic diblock copolymer CTA-*b*-PBLG.

Synthesis of C2TA-*b*-PBLG (8) and CTA-*b*-PBLG (9) via copper-catalyzed azide–alkyne cycloaddition (CuAAC) between azido-functionalized C2TA-N_3 (3)/CTA-N_3 (4) and alkyne-functionalized PBLG (7)

Proton NMR experiments of PBLGs (**7-1**) and (**7-2**) measured in $CDCl_3$ containing 15 % TFA revealed that the DP_ns of alkyne-functionalized PBLGs (**7-1**) and (**7-2**) were 26.6 and 47.1, respectively (See Supporting Information: the ^{1}H-NMR spectra of compounds **7-1** and **7-2** are shown in Figures S2 and S4, respectively).

To confirm the reactivity of CuAAC, azido-functionalized C2TA-N_3 (**3**), as a model cellulose derivative with low molecular weight, was coupled with alkyne-functionalized PBLG (**7-1**), resulting in the synthesis of diblock copolymer C2TA-*b*-PBLG (**8**) with a DP_n of PBLG 53.8, as confirmed by ^{1}H-NMR measurements in $CDCl_3$ (see Supporting Information: the ^{1}H-NMR spectrum of compound **8** is shown in Figure S3). The molecular weight of compound **8** was also underestimated by GPC analysis (chloroform as an eluent) likely because C2TA-*b*-PBLG (**8**) aggregates in chloroform and part of polymer, including the PBLG segment, was probably removed when filtering the solution (pore size: 2.7 μm) or by the guard column. Contrary to the low reactivity of CTA-NH_2 (**2**) as a macroinitiator for the ROP of BLG NCA (**5**),

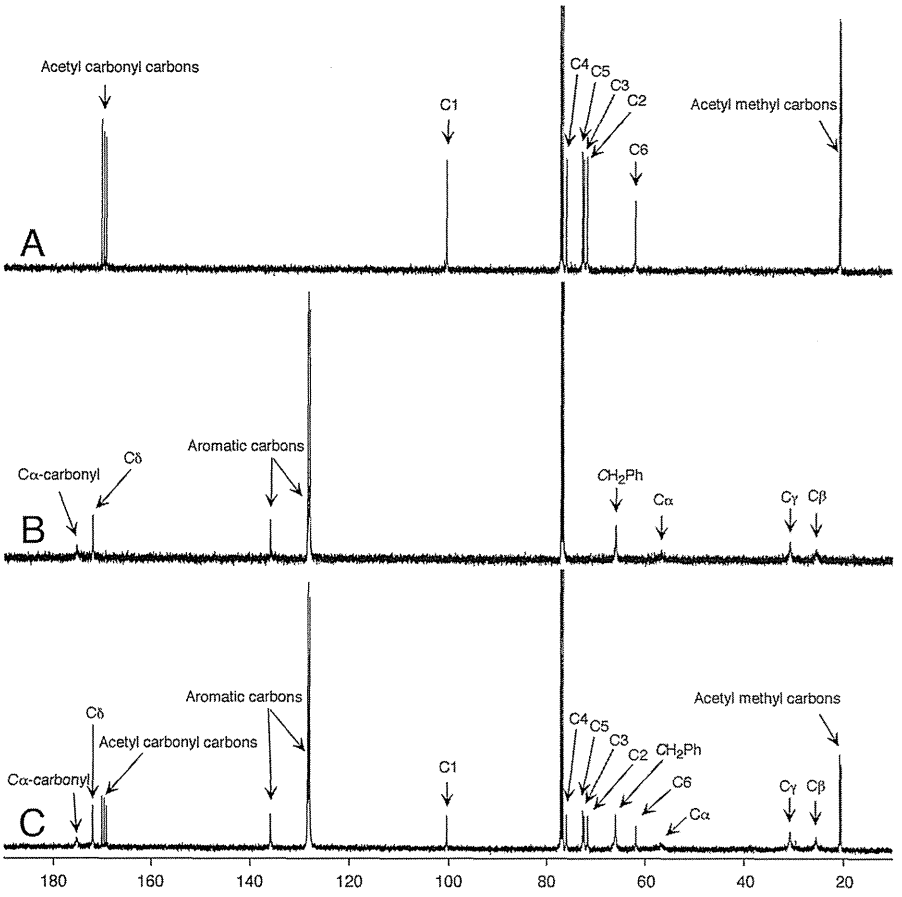

Fig. 2 ^{13}C NMR spectra of **A** azido-functionalized cellulose triacetate (**4**), **B** alkyne-functionalized PBLG (**7-2**), and **C** CTA-*b*-PBLG (**9**)

the azido group at the end of CTA showed a relatively high reactivity, and CuAAC between CTA-N_3 (**4**) and PBLG (**7-2**) proceeded successfully to produce CTA-*b*-PBLG (**9**). Because the GPC analysis of the diblock copolymer (**9**) exhibited a smaller molecular weight compared to the starting CTA-N_3 (**4**), we were unable to evaluate the DPs of both the CTA and PBLG segments of the resulting diblock copolymer CTA-*b*-PBLG (**9**). The hydrodynamic diameter of the alkyne-functionalized PBLG gradually increased with increasing time after its dissolution in $CHCl_3$, indicating that PBLG gradually aggregated in $CHCl_3$, as confirmed by dynamic light scattering experiments (data not shown). During GPC analysis, part of polymer, including the PBLG segment, was probably removed when filtering the solution (pore size: 0.45 μm) or by the guard column. Proton NMR analysis afforded a reasonable DP_n value for PBLG of 68.8 of CTA-*b*-PBLG (**9**), which was calculated based on the supposition that the DP_n of the CTA segment in CTA-*b*-PBLG (**9**) is 41.6.

Structure determination of CTA-*b*-PBLG (**9**)

Figure 1 shows the ^1H-NMR spectra of (A) azido end-functionalized CTA (**4**), (B) alkyne end-functionalized PBLG (**7-2**), and (C) CTA-*b*-PBLG (**9**) measured in $CDCl_3$. All protons of CTA-N_3 (**4**) were assigned as shown in Fig. 1a. The anomeric proton at the reducing-end of CTA-N_3 (**4**) appears at 4.60 ppm as a trace of a doublet ($J = 9.0$ Hz). Figure 1b shows broad proton resonances appearing at 3.94, 2.27, and 2.60 ppm, which were assigned to Hα, Hβ, and Hγ of the alkyne-functionalized PBLG (**7-2**), respectively. Although the protons resonances of the propargyl residues overlapped with those of the PBLG residues or could not be measured in $CDCl_3$ due to the aggregation of PBLG in chloroform, the methylene protons of the propargyl residue readily appear at 3.95 ppm (Wang et al. 2008) in a ^1H-NMR spectrum of propargyl-terminated PBLG (**7-2**) recorded in $CDCl_3$ containing 15 % TFA (Agut et al. 2008) (See Supporting Information: the ^1H-NMR spectrum of

compound **7-2** is shown in Figure S4). Using the NMR spectrum, we calculated the number-averaged degree of polymerization (DP_n) of the alkyne end-functionalized PBLG (**7**) as shown in Table 2. In Fig. 1c, the proton resonances of the CTA and PBLG segments of the diblock copolymer CTA-*b*-PBLG (**9**) appear as relatively broad signals. A weak resonance assigned to a proton at position 5 of a 1,4-disubstituted 1,2,3-triazole product appeared at 8.01 ppm as a singlet, indicating that CuAAC between azido-functionalized CTA (**4**) and alkyne-functionalized PBLG (**7-2**) proceeded successfully.

Figure 2 shows the ^{13}C-NMR spectra of (A) azido end-functionalized CTA (**4**), (B) alkyne end-functionalized PBLG (**7-2**), and (C) CTA-*b*-PBLG (**9**) measured in $CDCl_3$. The carbon resonance of C1 at the reducing end of the CTA residue could not be assigned, though all the protons of the CTA internal residues appeared, as shown in Fig. 2a. The Cβ, Cγ, and Cα carbons, as well as the two carbonyl carbons Cδ=O and Cα-C=O of alkyne end-functionalized PBLG (**7-2**), appeared at 25.5, 30.9, 56.8, 172.0, and 175.3 ppm, respectively, although the carbon resonances of the propargyl end group could not be found. MALDI-TOF MS analysis of the alkyne end-functionalized PBLG (**7-2**) confirmed that propargylamine initiated the ROP of PBLG. As shown in Fig. 2c, the internal residues of both the CTA and PBLG segments appeared and were assigned.

Figure 3 shows the infrared spectra of (A) tri-*O*-acetylcellulosylazide (**4**), (B) alkyne-functionalized PBLG (**7-2**), and (C) CTA-*b*-PBLG (**9**). Although the absorption of the azido group appeared at 2,120 cm^{-1} in spectrum (A), no absorption band was observed at the same wavenumber in spectrum (C). This means

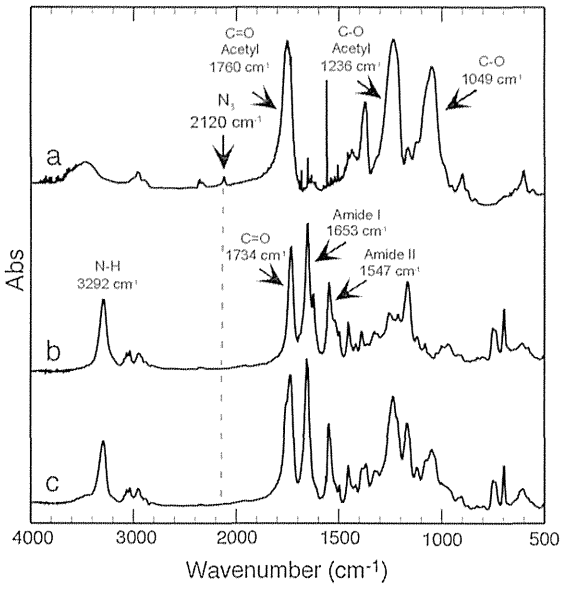

Fig. 3 Infrared spectra of **a** azido-functionalized cellulose triacetate (**4**), **b** alkyne-functionalized PBLG (**7-2**), and **c** CTA-*b*-PBLG (**9**)

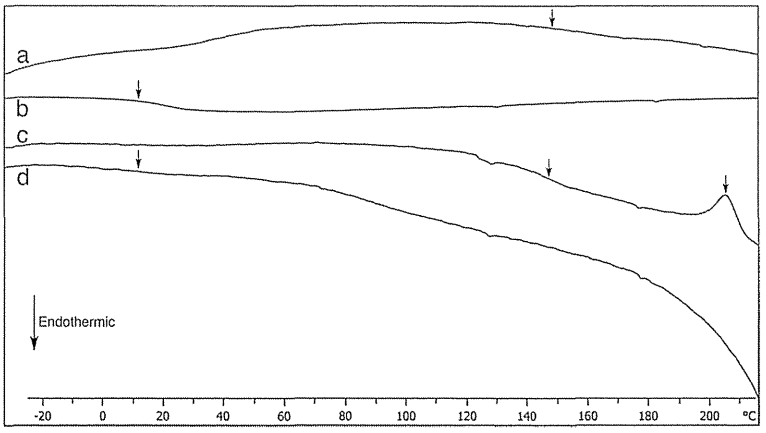

Fig. 4 Differential scanning calorimetry thermograms of **a** azido-functionalized cellulose triacetate (**4**) (2nd heating scan up to 290 °C), **b** alkyne-functionalized PBLG (**7-2**) (1st heating scan up to 290 °C after three heating scans up to 210 °C), **c** CTA-*b*-PBLG (**9**) (2nd heating scan up to 290 °C after three heating scans up to 210 °C and one heating scan up to 290 °C), and **d** CTA-*b*-PBLG (**9**) (1st heating scan up to 290 °C after three heating scans up to 210 °C). Heating rate: 5 °C/min; cooling rate: −50 °C/min; heating cycle: −40 to 210 °C three times, then −40 to 290 °C three times

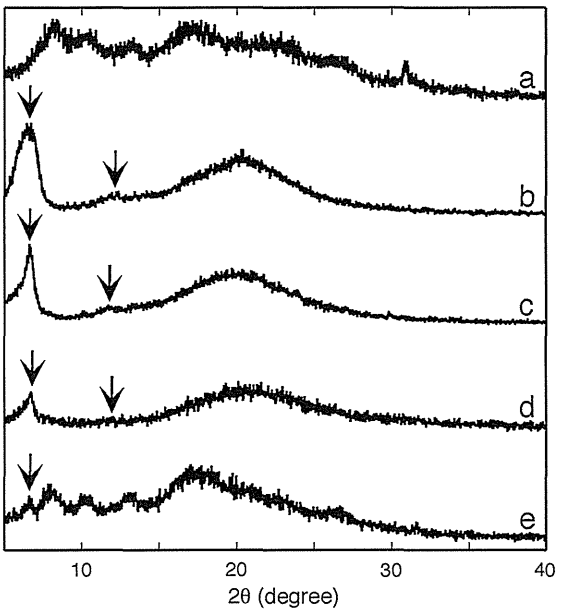

Fig. 5 Wide angle X-ray diffractograms of **a** azido-functionalized cellulose triacetate (**4**) with a CTA-II crystal structure before annealing, **b** alkyne-functionalized PBLG (**7-2**) before annealing, **c** PBLG (**7-2**) after annealing at 180 °C for 24 h, **d** CTA-*b*-PBLG (**9**) before annealing, and **e** CTA-*b*-PBLG (**9**) after annealing at 180 °C for 24 h

that CuAAC proceeded completely and that no CTA-N_3 (**4**) remained after the purification process.

The amide I and II bands appeared at 1,653 and 1,547 cm^{-1}, respectively, both in spectra b and c. The IR spectrum (c) shows that CTA-*b*-PBLG (**9**) contains both CTA and PBLG segments. The characteristic absorption band of the C=O group at 1,734 cm^{-1} and that of the acetyl carbonyl group at 1,760 cm^{-1} overlap in the spectrum of CTA-*b*-PBLG (**9**). The amide I band at 1,653 cm^{-1} indicates that PBLG exhibits an α-helix structure (Miyazawa 1960; Chirgadze and Brazhnikov 1974; Chirgadze et al. 1976; Lopez-Carrasquero et al. 1995) before annealing over the T_g of CTA, as described later.

Crystallization-induced microphase separation of CTA-*b*-PBLG (**9**)

Figure 4 shows the DSC curves of (a) azido-functionalized CTA (**4**), (b) alkyne-functionalized PBLG (**7-2**), and (c) and (d) CTA-*b*-PBLG (**9**). The glass transition temperatures (T_g) of CTA-N_3 (**4**) appeared at 144 °C, as shown in curve (a). The T_g of CTA with a low DP is known to appear at relatively low temperature (Kamitakahara et al. 2005). As shown in curve (b), T_g of the alkyne-functionalized PBLG (**7-2**) appeared at approx. 10 °C, which is comparable to previously reported values (Mckinnon and Tobolsky 1966; Koleske and Lundberg 1969; Watanabe and Uematsu 1984; Papadopoulos et al. 2004). In contrast, the T_gs of both the CTA and PBLG blocks appeared in diblock copolymer CTA-*b*-PBLG (**9**) in curves (c) and (d), respectively. Part of the alkyne-functionalized PBLG (**7-2**) presumably decomposed over 270 °C, because a large endothermic peak appeared in a first heating scan up to 290 °C. CTA-N_3 (**4**) showed a melting temperature (T_m) at 296 °C (heating rate: 10 °C/min), and an endothermic peak was observed from approx. 270 to 300 °C. Powders of CTA-N_3 (**4**), probably containing both amorphous phase and CTA-II crystals, were used for the DSC measurements, with the result being that T_g of CTA-N_3 (**4**) was not clearly observed in heating scans up to 210 °C, and then appeared in curve (a) after heating up to 290 °C, which is near the melting temperature of CTA-N_3 (**4**). Two separate T_gs of the CTA and PBLG blocks in the diblock copolymer CTA-*b*-PBLG (**9**) in one heating curve were unable to be observed, because the T_m of the CTA block is higher than or close to the decomposition temperature of the PBLG block. In addition, the cold crystallization temperature (T_c) of CTA-*b*-PBLG (**9**) was observed in a 2nd heating curve of CTA-*b*-PBLG (**9**) (c) at 205 °C. These facts indicate that the CTA and PBLG segments exist separately in the bulk.

The DSC data suggested that thermal treatment would enhance the microphase separation of CTA-*b*-PBLG (**9**). We therefore investigated the crystal structures of CTA-N_3 (**4**) and alkyne-functionalized PBLG (**7-2**) homopolymers and CTA-*b*-PBLG diblock copolymer (**9**) before and after annealing at 180 °C, which is higher than the T_g of CTA-*b*-PBLG (**9**), for 24 h by WAXD experiments. Figure 5 shows the WAXD profiles of CTA (**4**), PBLG (**7-2**), and CTA-*b*-PBLG (**9**). Figure 5a indicates that CTA has the CTA-II crystal structure even before annealing. PBLG exhibited an α-helix structure, as demonstrated by the appearance of diffractions (d = 13.4 Å and 7.4 Å: see arrows in Fig. 5b). Bragg reflections were found at scattering vectors with a ratio of $1:3^{1/2}$ at $2\theta = 6.62°$ (13.4 Å) and 11.2° (7.4 Å), indicating a

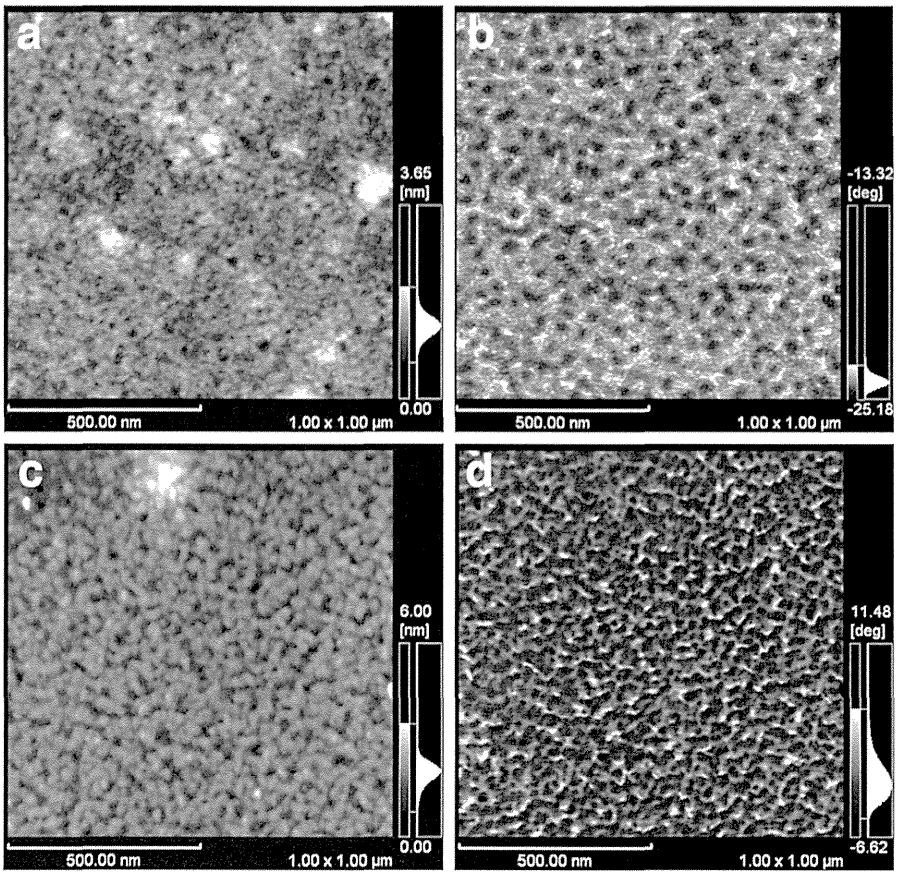

Fig. 6 Atomic force microscopy images of a CTA-*b*-PBLG thin film. Topographic images **a** before and **c** after annealing, respectively, and phase images **b** before and **d** after annealing, respectively

hexagonal columnar arrangement and 18/5 α-helical conformation of PBLG with a columnar diameter of 1.35 nm (Floudas et al. 2003; Zhou et al. 2010). After annealing, the crystallinity of the α-helix structure in PBLG (**7-2**) increased, as shown in Fig. 5c. In contrast, although an 18/5 α-helix structure of CTA-*b*-PBLG (**9**) appeared, no crystal structure was found in the CTA segment before annealing, as shown in Fig. 5d. The CTA-II crystal structure of the CTA segment in CTA-*b*-PBLG (**9**) appeared after annealing at 180 °C for 24 h as along with the α-helix structure of the PBLG segment, though the crystallinity of PBLG decreased. This phenomenon means that the CTA block separately crystallized in the bulk CTA-*b*-PBLG (**9**), causing the decrease in the α-helix structure in PBLG; it also strongly suggests that the thermal treatment, namely, the crystallization of CTA, enhanced the microphase separation between the CTA and PBLG segments at the molecular level, as described later.

Microphase separation of CTA-*b*-PBLG (9) as observed by AFM, FE-SEM and TEM

Oligopeptides of γ-benzyl-L-glutamate are known to form two secondary structures: α helices and β sheets stabilized by intra- and intermolecular hydrogen bonds, respectively (Papadopoulos et al. 2004). PBLG normally exhibits an α helix with an 18/5 helical conformation and a 0.54 nm spiral pitch, 3.6 residues per turn, affording 18 residues in five turns (Watanabe and Uematsu 1984). DP_n of the PBLG block of CTA-*b*-PBLG (**9**) was estimated as 68.8 by ^{1}H-NMR analysis. The length of the PBLG block was therefore calculated as 68.8/3.6 × 0.54 = 10.3 nm.

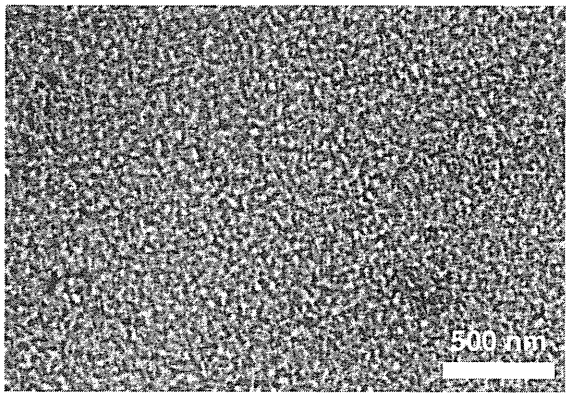

Fig. 7 Field emission scanning microscopy image by back scattering electron of a CTA-*b*-PBLG thin film, stained by ruthenium tetroxide. The color of the image was inverted for easy understanding of the image, comparable to those shown in Fig. 8. The image clearly shows the microphase separation of the dark parts (PBLG segments) and the bright layer (CTA segments)

Atomic force microscopy images of the thin film of CTA-*b*-PBLG are shown in Fig. 6. Both topographic and phase images changed after annealing at 180 °C for 24 h. In the phase image (b) before annealing, ellipsoidal particles with dimensions of about 15 nm for the semi-major axis and of circa 8 nm for the semi-minor one were detected. Those particles likely tend to orient in parallel. After the annealing process, both topological (c) and phase (d) images indicate that the film of CTA-*b*-PBLG (**9**) exhibits microphase separation. This fact is consistent with FE-SEM and TEM images of CTA-*b*-PBLG (**9**), as described later.

An inverted BSE image of the thin film of CTA-*b*-PBLG stained by RuO_4 vapor taken by FE-SEM is shown in Fig. 7. The image clearly indicates that the film of CTA-*b*-PBLG (**9**) exhibits microphase separation, and the dark parts stained by RuO_4 are likely PBLG segments. RuO_4 did not stain the CTA segments. The molecular length of $CTA_{41.6}$-*b*-$PBLG_{68.8}$ (**9**) was calculated as ca. 32.2 nm (21.9 nm (CTA) + 10.3 nm (PBLG α-helix)). The average thicknesses of the bright layer, CTA, and the dark layer, PBLG, were approx. 31 and 14 nm, respectively. The experimental data from FE-SEM is, therefore, likely consistent with the fact that the X-ray diffractogram of CTA-*b*-PBLG (**9**) displayed a CTA-II crystal structure, indicating anti-parallel packing of the CTA segments. The CTA segments

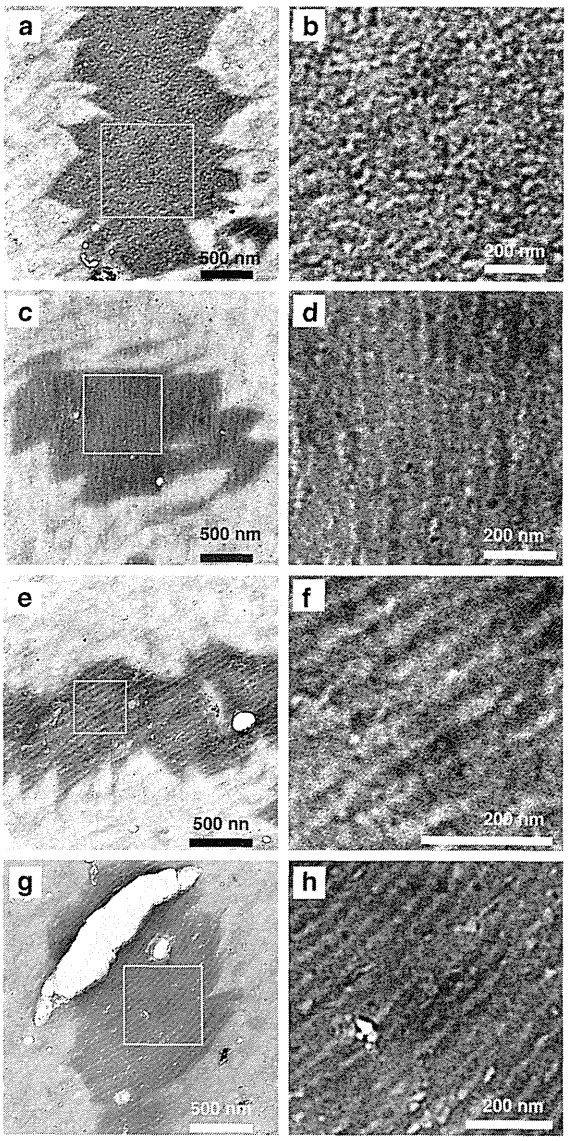

Fig. 8 Transmission electron microscopy images taken from ultrathin sections of CTA-*b*-PBLG (**9**) stained by ruthenium tetroxide vapor. Images **b**, **d**, **f**, and **h** are enlarged images from the square regions in **a**, **c**, **e**, and **g**, respectively. Microphase separation of the dark parts (PBLG segments) and bright layers (CTA segments) can be seen in different directions of ultrathin sectioning

probably interpenetrate or interdigitate in an anti-parallel direction to form bright ellipsoidal parts. The PBLG segments possibly produce double layers or an interpenetrated single layer of α-helices or random coils to afford the 14 nm thick dark part.

Transmission electron microscopy images of ultrathin sections of CTA-*b*-PBLG (**9**) are shown in Fig. 8.

Part of the bulk CTA-*b*-PBLG bulk was stained by RuO_4 vapor, likely because RuO_4 vapor was able to pass through holes in the diblock polymer bulk, and the polymers around the holes were preferentially stained. Microphase separation of the dark parts (PBLG segments) and bright layer (CTA segments) can be seen in different directions of the ultrathin sectioning (Fig. 8a, c, e, g). The morphologies of CTA-*b*-PBLG (**9**) shown in Fig. 8a, b are similar to those seen in the FE-SEM image in Fig. 7. In addition, characteristic lamellar-like morphologies were observed in Fig. 8c–h.

Bulk lamellar morphologies, including hexagon in lamella (HL) structure, have been investigated for peptide-containing copolymers as well (Papadopoulos et al. 2005; Sanchez-Ferrer and Mezzenga 2010). However, the present CTA-*b*-PBLG (**9**) formed different self-organization patterns. Thermal treatment over the T_g of CTA destroyed the hexagonal packing of PBLG, as demonstrated by the wide angle X-ray diffractograms, and preferentially induced CTA-crystallization-driven microphase separation. CTA possesses a CTA II crystal structure (space group: $P2_12_12_1$; dimensions $a = 24.68$ Å, $b = 11.52$ Å, and c (fiber axis) $= 10.54$ Å) (Roche et al. 1978; Dulmage 1957), and the distance between two CTA chains is shorter than that between two α helices of PBLG, probably resulting in the formation of a nearly amorphous structure of PBLG after annealing at 180 °C.

The nearly cylindrical (partly branched) morphology of the CTA portion is oriented nearly parallel in the polymer bulk, as shown in Figures c–h. A nearly spherical or partly ellipsoidal morphology of CTA-*b*-PBLG appears, as depicted in Fig. 8a, b, when the ultrathin section was sliced perpendicular to the direction of the cylindrical, partly branched CTA portion. The width of the bright and dark layers varies with the cutting angle to the direction of the cylindrical, partly branched CTA portion. The sizes of the bright and dark areas observed by TEM and FE-SEM were comparable.

Conclusions

We succeeded in the synthesis of well-defined CTA-*b*-PBLG via CuAAC, and we made the first observation of microphase separation of cellulosic materials in thin film and in bulk. The well-defined chemical structure of CTA-*b*-PBLG allowed us to build nanostructures of academic and practical interests. The crystallization-induced microphase separation by thermal treatment was key to produce the well-ordered nanostructure of the cellulosic diblock copolymer, CTA-*b*-PBLG. A more detailed investigation on the nanostructure of CTA-*b*-PBLG is of interest, and the preparation of CTA-*b*-PBLG with different lengths of the two segments will afford fundamental knowledge regarding the self-assembly of cellulosic diblock copolymers. This potent strategy for the preparation of microphase-separated cellulosic materials opens the door to new and valuable fields for cellulose such as medical applications and separation technologies. Moreover, our synthesis strategy is applicable to a wide range of cellulose esters such as cellulose diacetate (CDA) and cellulose ethers (Nakagawa et al. 2012), thereby producing diverse cellulosic diblock copolymers.

Acknowledgments We are indebted to Prof. Yoshiyuki Nishio of Kyoto University for the discussion on thermal analysis. We thank the Japan Society for the Promotion of Science (JSPS) for their financial support of this study, in part, through Grant-in-Aid for Scientific Research (nos. 21580205 and 24380092), and a Sekisui Chemical Grant Program for Research.

References

Agut W, Agnaou R, Lecommandoux S, Taton D (2008) Synthesis of block copolypeptides by click chemistry. Macromol Rapid Commun 29:1147–1155. doi:10.1002/Marc.200800123

Ando I, Yamada S, Sanefuji T, Shoji A, Uematsu I (1987) Effect of pressure on the molecular motion of a poly(γ-benzyl L-glutamate) lyotropic liquid crystal as studied by proton nuclear magnetic resonance. Polymer 28:716–720. doi:10.1016/0032-3861(87)90218-7

Caillol S, Lecommandoux S, Mingotaud A-F, Schappacher M, Soum A, Bryson N, Meyrueix R (2003) Synthesis and self-assembly properties of peptide-polylactide block copolymers. Macromolecules 36:1118–1124. doi:10.1021/ma021187c

Cao H, Yao J, Shao Z (2012) Synthesis of poly(γ-benzyl-L-glutamate) with well-defined terminal structures and its block polypeptides with alanine, leucine and phenylalanine. Polym Int 61:774–779. doi:10.1002/pi.4138

Ceresa RJ (1961) The synthesis of block and graft copolymer of cellulose and its derivatives. Polymer 2:213–219

Chen D (2013) Crystal behavior of semicrystalline polystyrene-block-poly(L-lactide) diblock copolymer in thin films with various structures. Polym Int 62:1343–1350. doi:10.1002/pi.4426

Chirgadze YN, Brazhnikov EV (1974) Intensities and other spectral parameters of infrared amide bands of polypeptides in the α-helical form. Biopolymers 13:1701–1712. doi:10.1002/bip.1974.360130902

Chirgadze YN, Brazhnikov EV, Nevskaya NA (1976) Intramolecular distortion of the α-helical structure of polypeptides. J Mol Biol 102:781–792. doi:10.1016/0022-2836(76)90291-6

Daly WH, Poche D (1988) The preparation of N-Carboxyanhydrides of alpha-amino-acids using bis(trichloromethyl)carbonate. Tetrahedron Lett 29:5859–5862. doi:10.1016/S0040-4039(00)82209-1

de Oliveira W, Glasser WG (1994) Multiphase materials with lignin 13. Block-copolymers with cellulose propionate. Polymer 35:1977–1985

Dulmage WJ (1957) The molecular and crystal structure of cellulose triacetate. J Polym Sci 26:277–288. doi:10.1002/Pol.1957.1202611402

Edgar KJ, Buchanan CM, Debenham JS, Rundquist PA, Seiler BD, Shelton MC, Tindall D (2001) Advances in cellulose ester performance and application. Prog Polym Sci 26:1605–1688. doi:10.1016/S0079-6700(01)00027-2

Enomoto Y, Kamitakahara H, Takano T, Nakatsubo F (2006) Synthesis of diblock copolymers with cellulose derivatives. 3. Cellulose derivatives carrying a single pyrene group at the reducing-end and fluorescent studies of their self-assembly systems in aqueous NaOH solutions. Cellulose 13:437–448

Enomoto-Rogers Y, Kamitakahara H, Yoshinaga A, Takano T (2011) Synthesis of diblock copolymers with cellulose derivatives 4. Self-assembled nanoparticles of amphiphilic cellulose derivatives carrying a single pyrene group at the reducing-end. Cellulose 18:1005–1014. doi:10.1007/S10570-011-9549-4

Farrar D, Yu MS, West JE, Moon W (2010) Piezoelectric biopolymer-polymer composite films and microfibers. Johns Hopkins APL Tech Dig 28:258–259

Feger C, Cantow HJ (1980) Cellulose containing block copolymers 1. Synthesis of trimethylcellulose-(b-poly(oxytetramethylene))-star block copolymers. Polym Bull 3:407–413

Floudas G, Papadopoulos P, Klok HA, Vandermeulen GWM, Rodriguez-Hernandez J (2003) Hierarchical self-assembly of poly(gamma-benzyl-L-glutamate)-poly(ethylene glycol)-poly(gamma-benzyl-L-glutamate) rod-coil-rod triblock copolymers. Macromolecules 36:3673–3683. doi:10.1021/Ma025918k

Habraken GJM, Wilsens KHRM, Koning CE, Heise A (2011) Optimization of N-carboxyanhydride (NCA) polymerization by variation of reaction temperature and pressure. Polym Chem 2:1322–1330. doi:10.1039/C1py00079a

Hiratsuka N, Shiba K, Shinomura K, Hosaki S, Cho H, Nagasaki A, Kobayashi S (1994) Urinary protein-fractions in healthy-subjects using cellulose-acetate membrane electrophoresis followed by staining with acid-violet-17. Biol Pharm Bull 17:1355–1357

Howell B, Reneker DH (1990) Morphology of polymer-films and single molecules. J Appl Polym Sci 40:1663–1682. doi:10.1002/App.1990.070400921

Ibarboure E, Papon E, Rodriguez-Hernandez J (2007) Nanostructured thermotropic PBLG–PDMS–PBLG block copolymers. Polymer 48:3717–3725. doi:10.1016/j.polymer.2007.04.046

Jadage CD, Lonikar SV, Wadgaonkar PP (2004) Starch and cellulose based graft and block copolymers. In: Society for polymer science, India, pp PD.1/1–PD.1/5

Kadokawa J-I, Karasu M, Tagaya H, Chiba K (1996) Synthesis of a block copolymer consisting of oligocellulose and oligochitin. J Macromol Sci, Pure Appl Chem A33:1735–1743. doi:10.1080/10601329608010937

Kamatani A, Kikuchi Y (2002) Carbohydrate diblock and triblock copolymers with desirable molecular weights and their manufacture. JP2002146025A,

Kamitakahara H, Nakatsubo F (2005) Synthesis of diblock copolymers with cellulose derivatives. 1. Model study with azidoalkyl carboxylic acid and cellobiosylamine derivative. Cellulose 12:209–219

Kamitakahara H, Enomoto Y, Hasegawa C, Nakatsubo F (2005) Synthesis of diblock copolymers with cellulose derivatives. 2. Characterization and thermal properties of cellulose triacetate-block-oligoamide-15. Cellulose 12:527–541

Kang IK, Ito Y, Sisido M, Imanishi Y (1988) Gas permeability of the film of block and graft copolymers of polydimethylsiloxane and poly(gamma-benzyl L-glutamate). Biomaterials 9:349–355

Kim S, Stannett VT, Gilbert RD (1973) A new class of biodegradable polymers. J Polym Sci Polym Lett 11:731–735

Kim S, Stannett VT, Gilbert RD (1976) Biodegradable cellulose block copolymers. J Macromol Sci Pt A Chem A10:671–679

Koleske JV, Lundberg RD (1969) Secondary transitions in poly(γ-benzyl-L-glutamate) and in poly(γ-benzyl-DL-glutamate). Macromolecules 2:438–440. doi:10.1021/ma60010a024

Kubota R, Machii R, Hiratsuka N, Hotta O, Itoh Y, Kobayashi S, Shiba K (2003) Cellulose acetate membrane electrophoresis in the analysis of urinary proteins in patients with tubulointerstitial nephritis. J Clinic Lab Anal 17:44–51. doi:10.1002/Jcla.10066

Lonikar SV, Gilbert RD, Fornes RE, Stejskal E (1990) Block copolymers of polysaccharides and polyamino acids. Abstracts of papers of the American Chemical Society 199:364-POLY

Lopez-Carrasquero F, Aleman C, Munoz-Guerra S (1995) Conformational analysis of helical poly(β-L-aspartate)s by IR dichroism. Biopolymers 36:263–271

Machii R, Kubota R, Hiratsuka N, Sugimoto K, Masudo R, Kurihara Y, Kobayashi S, Shiba K (2004) Urinary protein fraction in healthy subjects using cellulose acetate membrane electrophoresis followed by colloidal silver staining. J Clinic Lab Anal 18:231–236. doi:10.1002/Jcla.20028

Machii R, Sakatume M, Kubota R, Kobayashi S, Gejyo F, Shiba K (2005) Examination of the molecular diversity of alpha(1) antitrypsin in urine: deficit of an alpha(1) globulin fraction on cellulose acetate membrane electrophoresis. J Clinic Lab Anal 19:16–21. doi:10.1002/Jcla.20049

Mckinnon AJ, Tobolsky AV (1966) Structure and transition in solid state of a helical macromolecule. J Phys Chem 70:1453. doi:10.1021/J100877a018

Mezger T, Cantow HJ (1983a) Cellulose containing block copolymers.4. Cellulose triester macroinitiators. Angew Makromol Chem 116:13–27

Mezger T, Cantow HJ (1983b) Cellulose containing block co-polymers. 5. Threeblock co-polymer syntheses via macroinitiator. Makromol Chem, Rapid Commun 4:313–320

Mezger T, Cantow HJ (1984) Cellulose-containing triblock copolymers—syntheses via cellulosic dithiodiaryl photoinitiators. Polym Photochem 5:49–56

Miyazawa T (1960) Perturbation treatment of the characteristic vibrations of polypeptide chains in various configurations. J Chem Phys 32:1647–1652. doi:10.1063/1.1730999

Nakagawa A, Kamitakahara H, Takano T (2012) Synthesis and thermoreversible gelation of diblock methylcellulose analogues via Huisgen 1,3-dipolar cycloaddition. Cellulose 19:1315–1326. doi:10.1007/S10570-012-9703-7

Papadopoulos P, Floudas G, Klok HA, Schnell I, Pakula T (2004) Self-assembly and dynamics of poly(γ-benzyl-L-glutamate) peptides. Biomacromolecules 5:81–91. doi:10.1021/bm034291q

Papadopoulos P, Floudas G, Schnell I, Aliferis T, Iatrou H, Hadjichristidis N (2005) Nanodomain-induced chain folding in poly(gamma-benzyl-L-glutamate)-b-polyglycine diblock copolymers. Biomacromolecules 6:2352–2361. doi:10.1021/Bm0501860

Pohjola L, Eklund V (1977) Polyurethane block copolymers from cellulose acetate. Pap Puu 3:117–120

Roche E, Chanzy H, Boudeulle M, Marchessault RH, Sundararajan P (1978) 3-dimensional crystalline-structure of cellulose triacetate-ii. Macromolecules 11:86–94. doi:10.1021/Ma60061a016

Sakaguchi M, Ohura T, Iwata T, Takahashi S, Akai S, Kan T, Murai H, Fujiwara M, Watanabe O, Narita M (2010) Diblock copolymer of bacterial cellulose and poly(methyl methacrylate) initiated by chain-end-type radicals produced by mechanical scission of glycosidic linkages of bacterial cellulose. Biomacromolecules 11:3059–3066. doi:10.1021/Bm100879v

Sanchez-Ferrer A, Mezzenga R (2010) Secondary structure-induced micro- and macrophase separation in rod-coil polypeptide diblock, triblock, and star-block copolymers. Macromolecules (Washington DC, U S) 43:1093–1100. doi:10.1021/ma901951s

Sanefuji T, Ando I, Inoue Y, Uematsu I, Shoji A (1985) Effect of pressure on the magnetic orientation of the poly(γ-benzyl L-glutamate) liquid crystal as studied by proton NMR under high pressure. Macromolecules 18:583–585. doi:10.1021/ma00145a048

Toriumi H, Uematsu I (1984) Optical properties of lyotropic poly(γ-benzyl L-glutamate) liquid crystals. Mol Cryst Liq Cryst 116:21–33. doi:10.1080/00268948408072493

Toriumi H, Kusumi Y, Uematsu I, Uematsu Y (1979) Thermally induced inversion of the cholesteric sense in lyotropic polypeptide liquid crystals. Polym J 11:863–869. doi:10.1295/polymj.11.863

Toriumi H, Minakuchi S, Uematsu Y, Uematsu I (1980) Helical twisting power of poly(γ-benzyl L-glutamate) liquid crystals in mixed solvents. Polym J (Tokyo) 12:431–437. doi:10.1295/polymj.12.431

Toriumi H, Minakuchi S, Uematsu I (1981) Concentration and temperature dependence of the helical twisting power of poly(γ-benzyl L-glutamate) liquid crystals in m-cresol. J Polym Sci Polym Phys Ed 19:1167–1169. doi:10.1002/pol.1981.180190715

Toriumi H, Yahagi K, Uematsu I, Uematsu Y (1983) Cholesteric structure of lyotropic poly(γ-benzyl L-glutamate) liquid crystals. Mol Cryst Liq Cryst 94:267–284. doi:10.1080/15421408308084262

Trent JS, Scheinbeim JI, Couchman PR (1983) Ruthenium tetraoxide staining of polymers for electron-microscopy. Macromolecules 16:589–598. doi:10.1021/Ma00238a021

Tsai ML, Chen SH, Marshall KL, Jacobs SD (1990) Thermotropic and optical properties of chiral nematic polymers. Int J Thermophys 11:213–223. doi:10.1007/bf00503872

Uematsu I, Uematsu Y (1984) Polypeptide liquid crystals. Adv Polym Sci 59:37–73

Vivatpanachart S, Tsujita Y, Takizawa A (1981) Gas permeability of the racemic form of poly(γ-benzyl glutamate). Makromol Chem 182:1197–1206

Wang K, Liang LY, Lin SL, He XH (2008) Synthesis of well-defined ABC triblock copolymers with polypeptide segments by ATRP and click reactions. Eur Polym J 44:3370–3376. doi:10.1016/J.Eurpolymj.07.042

Watanabe J, Uematsu I (1984) Anomalous properties of poly(γ-benzyl L-glutamate) film composed of unusual 7/2 helices. Polymer 25:1711–1717. doi:10.1016/0032-3861(84)90242-8

Weiss RA, Shao L, Lundberg RD (1992) Melt-processable polypeptide/ionomer molecular composites. Macromolecules 25:6370–6372. doi:10.1021/ma00049a039

Yagi S, Kasuya N, Fukuda K (2010) Synthesis and characterization of cellulose-b-polystyrene. Polym J (Tokyo, Jpn) 42:342–348. doi:10.1038/pj.2009.342

Zhou QH, Zheng JK, Shen ZH, Fan XH, Chen XF, Zhou QF (2010) Synthesis and hierarchical self-assembly of rod rod block copolymers via click chemistry between mesogen-jacketed liquid crystalline polymers and helical polypeptides. Macromolecules 43:5637–5646. doi:10.1021/Ma1007418

Carbohydrate Polymers 113 (2014) 279–285

Contents lists available at ScienceDirect

Carbohydrate Polymers

journal homepage: www.elsevier.com/locate/carbpol

Facile synthesis of acyl chitosan isothiocyanates and their application to porphyrin-appended chitosan derivative

Masaya Shibano, Shouko Nishida, Yasuko Saito, Hiroshi Kamitakahara, Toshiyuki Takano *

Division of Forest and Biomaterials Science, Graduate School of Agriculture, Kyoto University, Kyoto, Japan

ARTICLE INFO

Article history:
Received 27 March 2014
Received in revised form 21 May 2014
Accepted 30 May 2014
Available online 14 July 2014

Keywords:
Acylation
Chitosan
Isothiocyanate
N-Phenylthiocarbamoylation
Photocurrent
Porphyrin

ABSTRACT

Chitosan (**1**) was reacted with phenylisothiocyanate in 5% AcOH/H_2O to give *N*-phenylthiocarbamoyl chitosan (**2**) with a degree of substitution (DS) of *N*-phenylthiocarbamoyl groups of 0.86 in 87.1% yield. The following acylation of compound **2** with hexanoyl chloride in the presence of pyridine afforded 3,6-di-*O*-2,3-hexanoyl chitosan isothiocyanate (**4a**) with a DS of the isothiocyanate groups of 0.70 in high yield, unexpectedly. Compound **4a** exhibited high levels of reactivity toward various amines to give the corresponding *N*-thiocarbamoyl chitosan derivatives in high yields. Other acyl (decanoyl (**4b**), myristroyl (**4c**), stearoyl (**4d**), benzoyl (**4e**)) chitosan isothiocyanates were also prepared from chitosan (**1**) in high yields. To evaluate the potential applications of acyl chitosan isothiocyanates, *N*-(triphenylporphynyl)thiocarbamoyl chitosan derivative **6** with a DS of the triphenylporphynyl groups of 0.46 was prepared from compound **4b**. The Langmuir–Blodgett monolayer film of compound **6** gave a good photon-to-electron conversion performance.

1. Introduction

Chitosan is a linear cationic heteropolymer of *N*-acetylglucosamine (GlcNAc) and glucosamine (GlcN) residues thorough β-1,4 linkages by the deacetylation of chitin which is the second most abundant natural biopolymer in nature, and a most versatile polysaccharide that lends itself to countless chemical and biochemical modifications (Harish Prashanth & Tharanathan, 2007; Kurita, 2006; Mouya & Inamdar, 2008; Muzzarelli & Muzarelli, 2005; Muzzarelli, Tosi, Francescangeli & Muzzarelli 2003; Ravi Kumar, Muzzarelli, Muzzarelli, Sashiwa, & Domb, 2004; Rinaudo, 2006; Sahoo, Sahoo, Mohanty, Sasmal, & Nayak, 2009). However, considerable levels of attention have still been focused on the development of the high-value-added utilization for chitosan and its derivatives.

The *N*-substituted thiocarbamoyl chitosan derivatives which was prepared by *N*-thiocarbamoylation of chitosan with isothiocynate compounds are one of the important functional chitosan derivatives. For example, *N*-acetyl- (Fekry & Mohamed, 2010), *N*-acyl- (Zhong et al., 2008), *N*-fluoresceinyl- (Ma et al., 2008; Qaqish & Amiji, 1999), *N*-phenyl- (Baba, Noma, Nakayama & Matsushita, 2002, Monier & Abdel-Latif, 2012) thiocarbamoyl chitosan derivatives has been reported as a corrosion inhibitor, an antimicrobial material, a macromolecular fluorophore, a metal adsorbent, respectively. However, the availability of the commercial isothiocyanate compounds are limited. If chitosan isothiocyanate derivatives are easily synthesized, various amines are available for the syntheses of versatile *N*-substituted thiocarbamoyl chitosan derivatives for new applications. Glucosamine isothiocyanate derivatives can be prepared by the reaction of glucosamine with thiophosgene (Fernández-Bolaños, Zafra, López, Robina & Fuentes, 1999; Jochims & Seegler, 1965), but similar chitosan isothiocyanate derivatives have not been reported in the literature, even though chitosan has an amino group at its C-2 position that could be converted to an isothiocyanate group. The isothiocyanation of amines can be achieved by the reaction of an amine with thiophosgene or carbon disulfide (Fernández & Mellet, 1999, Munch, Hansen, Pittelkow, Christensen & Boas, 2008; Mukerjee & Ashare, 1991; Sun, Hu, Zhao, & Liu, 2012; Sun, Li, et al., 2012), although it is important to mention that both of these reagents are highly toxic. With this in mind, the development of a facile and safe synthetic method for the formation of chitosan isothiocyanate derivatives is strongly desired.

We recently reported a facile and safe synthetic method for acyl chitosan isothiocyanates by two reactions, that is, *N*-phenylthiocarbamoylation with phenylisothiocyanate and

* Corresponding author at: Division of Forest and Biomaterials Science, Graduate School of Agriculture, Kyoto University, Sakyo-ku, Kyoto 606-8502, Japan.
Tel.: +81 75 753 6254; fax: +81 75 753 6300.
E-mail address: takatmys@kais.kyoto-u.ac.jp (T. Takano).

http://dx.doi.org/10.1016/j.carbpol.2014.05.099
0144-8617/

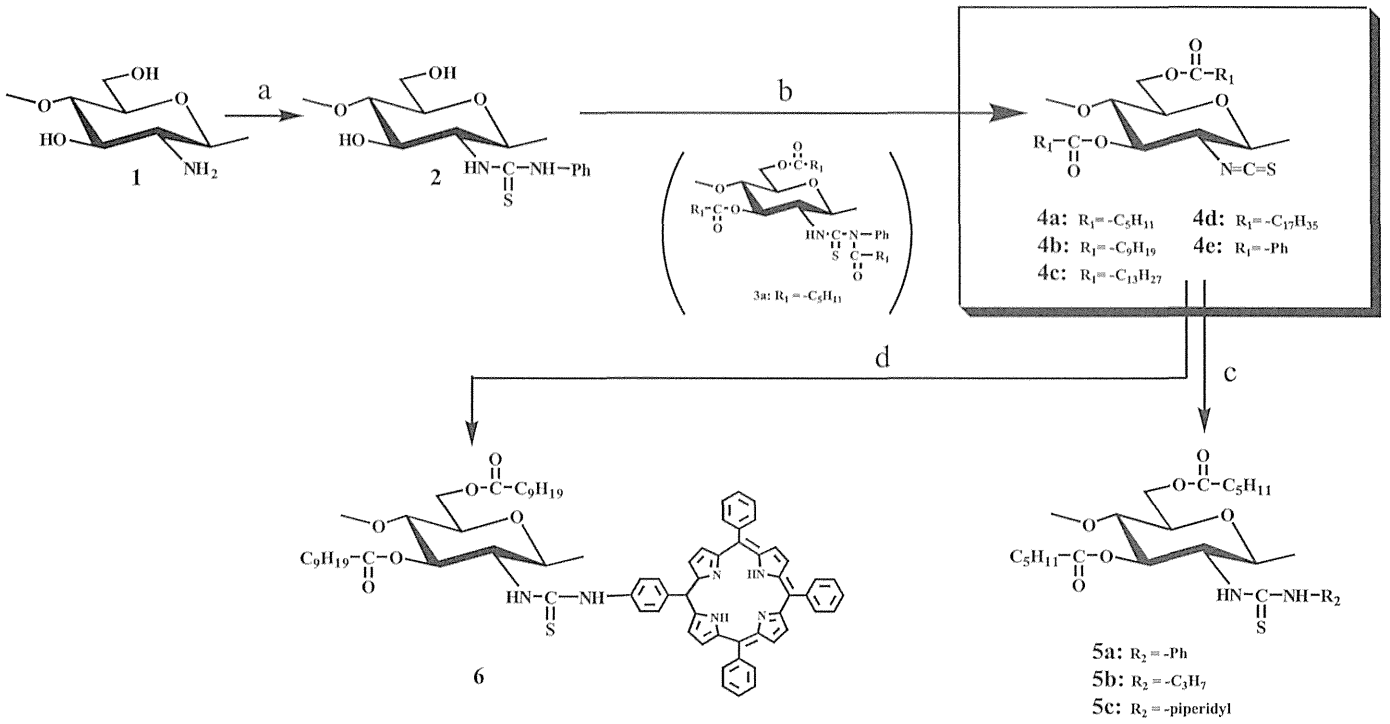

a) Ph-N=C=S/ 5%-AcOH/H_2O/ MeOH, 30°C, 48 h ; b) Acyl chloride/ Pyridine / $CHCl_3$, 1°C, 1h → 30°C, 1 h→ 80°C, 18 h
c) Amine/ THF, 35°C, 48 h; d) TPP-NH_2/ CH_2Cl_2, 35°C, 48 h

Scheme 1. Preparation of *N*-substituted thiocarbamoyl chitosan derivatives (**5a–c** and **6**) via the corresponding acyl chitosan isothiocyanates (**4a–e**).

acylation with acyl halide or acyl anhydride (Takano & Shibano, 2013). The resulting acyl chitosan isothiocyanates are soluble in common organic solvents and are expected to be useful synthetic intermediates for new functional chitosan derivatives. But, we did not report this procedure in its full detail.

On the other hand, the synthesis of porphyrin-containing chitosan derivatives represents one of several recent proposals for the high-value-added utilization of chitosan, with other examples including the construction of metallotetraphenylporphyrin appended chitosan derivatives (Huang, Guo & Tang, 2007), the use of an Mn(III) deuteroporphyrin-bearing chitosan as catalyst for oxidation reactions (Sun, Hu, et al., 2012), and tetraphenylporphyrin tethered chitosan derivatives for use as nanocarriers for gene delivery (Gaware et al., 2013). The LB monolayer films of 6-*O*-porphynyl-2,3-di-*O*-stearoyl cellulose, which is a regioselectively substituted cellulose derivative, have been reported to exhibit high photon-to-electron conversion performances (Sakakibara, Ogawa & Nakatsubo, 2007). The high performance of this material has been attributed to the dense packing of the porphyrin moieties along the cellulose backbone because of the well-defined and regular structure of the cellulose derivative. The *N*-porphynylthiocarbamoyl chitosan derivatives prepared from the acyl chitosan isothiocyanates could therefore potentially be used as alternative photon-to-electron conversion materials.

This paper provides a detailed account of our new method for the synthesis of acyl chitosan isothiocyanates (Scheme 1). Furthermore, we have described the reactivity of these materials with various amines, and the preparation and evaluation of an LB monolayer film of porphyrin-appended chitosan derivative as one of the examples of the application of the isothiocyanates for the preparation of functional chitosan derivatives.

2. Experimental

2.1. General

Chitosan (DAICHITOSAN 100D (VL), degree of deacetylation 98%) was kindly supplied by Dainichiseika Color & Chemicals Manufacturing Co. (Tokyo, Japan). All of the other chemicals used in the study were purchased from commercial sources and used without further purification. Fourier-transform-infrared (FT-IR) spectra were recorded on a Shimadzu IR Prestige-21 spectrophotometer (Shimadzu, Kyoto, Japan) as KBr pellets (sample 1 mg/KBr 200 mg). ^1H and ^{13}C NMR were recorded on a Varian 500 MHz FT-NMR spectrophotometer (Aglient Technologies, Santa Clara, CA, USA) using tetramethylsilane (TMS) as an internal reference standard in DMSO-d_6 or $CDCl_3$. The standard number of scans in the ^1H and ^{13}C NMR measurements were 3500 and 22,000, respectively. The chemical shifts (δ) of the NMR spectra have been reported in parts per million (ppm). UV–vis spectra were recorded on a Jasco V-560 UV–vis spectrophotometer (Jasco, Tokyo, Japan).

2.2. Preparation of acyl chitosan isothiocyanate

2.2.1. N-Phenylthiocarbamoylation

Chitosan (**1**, 1.20 g, 7.45 mmol) was dissolved in a 5% (v/v) solution of AcOH in water (30 mL) and the resulting solution was diluted with MeOH (120 mL). Phenyl isothiocyanate (5.34 mL, 44.7 mmol) was then added to the solution, and the resulting mixture was stirred at 35 °C for 24 h, during which time a precipitate formed. The precipitate was filtered, and the filter-cake was washed with MeOH before being collected and suspended in MeOH (300 mL) without drying. The suspension was then stirred at ambient temperature for 30 min and filtered, and the filter-cake was washed with MeOH. This purification procedure was repeated several times until no

absorbance could be detected at 280 nm in the filtrate. The solid product was then dried in vacuo to afford *N*-phenylthiocarbamoyl chitosan (**2**, 1.80 g, 87.1% yield).

Compound **2** – DS $_{PhNHCS}$: 0.86 (determined by elemental analysis); FT-IR (KBr): ν 3298, 2873, 1660, 1541, 1497, 1373, 1234, 1150, 1065, 898, 746, 692 cm^{-1}; ^1H NMR (DMSO-d_6): δ 9.43 (NH), 7.80–7.00 (phenyl-H), 4.69 (H-1), 4.00–3.00 (H-2, H-3, H-4, H-5, H-6a, H-6b) ppm; ^{13}C NMR (DMSO-d_6): δ 182.0 (C=S), 139.5, 129.1, 124.5 (phenyl-C), 102.5 (C-1), 82.0 (C-4), 75.1 (C-5), 73.2 (C-3), 60.6 (C-6), 59.9 (C-2) ppm.

2.2.2. Acylation

*2.2.2.1. 3,6-Di-O-hexanoyl chitosan isothiocyanate (**4a**) (typical method).* Compound **2** (300 mg, 1.1 mmol) was suspended in a mixture of $CHCl_3$ (6 mL) and pyridine (10 mL), and the resulting suspension was stirred at 35 °C for 24 h. A solution of hexanoyl chloride (1.66 mL, 12.1 mmol) in $CHCl_3$ (4 mL) was then added to the suspension in a drop-wise manner at 0 °C over a period of 10 min. The resulting mixture was then stirred at 1–2 °C for 1 h before being heated at 30 °C for 1 h. The mixture was then heated at 80 °C for 18 h, before being cooled to ambient temperature and poured into MeOH (400 mL). The resulting mixture was stirred at ambient temperature for 2 h and formed a suspension, which was filtered. The filter-cake was then washed with MeOH before being collected and dissolved in a small amount of $CHCl_3$. The resulting solution was added to MeOH (400 mL) in a drop-wise manner to give a suspension, which was filtered. The filter-cake was then washed with MeOH before being collected and dried in vacuo to afford compound **4a** (409 mg).

Compounds **4b–e** were also prepared according to the procedure for compound **4a**. The DS, ^1H and ^{13}C NMR and FT-IR data of compounds **4a–e** were summarized in Table 1.

2.3. Reactivity of hexanoyl chitosan isothiocyanate *4a* with amines

*2.3.1. 3,6-Di-O-hexanoyl-N-phenylthiocarbamoyl chitosan (**5a**) (typical method)*

Aniline (0.23 mL, 2.50 mmol) was added to a solution of compound **4a** (200 mg) in THF (4 mL), and the resulting mixture was stirred at 35 °C for 24 h before being poured into distilled water (400 mL). The resulting precipitate was collected by filtration, and the filter-cake was washed with distilled water before being collected and dissolved in a small amount of THF. The resulting solution was added to distilled water (400 mL) in a drop-wise manner to give a precipitate, which was collected by filtration. The filter-cake was then washed with distilled water before being collected and dried in vacuo at 40 °C to afford compound **5a** (196 mg).

Compound **4a** was also reacted with *n*-propyl amine and piperidine by the same procedure to give compounds **5b** and **5c**. The DS, ^1H and ^{13}C NMR and FT-IR data of compounds **5a–c** were summarized in Table 1.

2.4. Application of decanoyl chitosan isothiocyanate (*4b*) to the formation of functional chitosan derivatives

*2.4.1. Preparation of 3,6-di-O-hexanoyl-N-(p-(10,15,20-triphenyl-5-porphyrinyl)phenyl) thiocarbamoyl chitosan (**6**)*

5-(4′-Aminophenyl)-10,15,20-triphenylporphyrin (TPP-NH_2) (29.1 mg), which was prepared according to the method reported by Luguya, Jaquinod, Fronczek, Vicente, & Smith (2004), was added to a solution of compound **4b** (30 mg) in CH_2Cl_2 (4 mL), and the resulting mixture was stirred at 35 °C for 48 h in the absence of light before being poured into MeOH (200 mL). The resulting precipitate

Table 1
Data of compounds **4a–e** and **5a–c**.

Compound (acyl group)	**4a** (hexanoyl)	**4b** (decanoyl)	**4c** (myristroyl)	**4d** (stearoyl)	**4e** (benzoyl)	**5a** (hexanoyl)	**5b** (hexanoyl)	**5c** (hexanoyl)
DS[a]	0.74 NCS	0.70 NCS	0.70 NCS	0.70 NCS	0.56 NCS	0.68 PhNHCS-	0.68 PrNHCS-	0.64 PiperidylNHCS-
^1H NMR (in $CDCl_3$) (ppm)								
H-3	5.18	5.17	5.17	5.17	5.22	5.03	5.10	5.01
H-1, H-6a	4.45	4.44	4.45	4.45	4.28	4.80–4.00	4.50–4.00	4.65–4.00
H-6b	4.26	4.26	4.27	4.26	4.09			
H-2, H-4, H-5	3.67	3.67	3.67	3.67	3.67	4.00–3.40	4.00–3.40	4.00–3.40
acyl —OCO*CH_2*—	2.37	2.35	2.38	2.35	–	2.30	2.34	2.34
acyl —OCOCH_2—*CH_2*—	1.65	1.64	1.64	1.60	–	1.58	1.62	1.61
acyl —*CH_2*—	1.34	1.27	1.26	1.26	–	1.29	1.32	1.32
acyl —*CH_3*	0.91	0.88	0.88	0.88	–	0.88	0.89	0.88
Others	–	–	–	–	8.17–7.67, 7.64–6.90 (benzoyl aromatic-H)	7.60–7.06 (phenyl aromatic-H)	2.34, 1.32, 0.89 (propyl-H)	2.60–2.20, 1.51 (piperidyl-H)
^{13}C NMR (in $CDCl_3$) (ppm)								
C=S	–	–	–	–	–	181.0	183.1	180.9
C=O	172.8, 172.3	172.8, 172.3	172.8, 172.2	172.8, 172.2	164.9, 164.8	173.5, 173.4	173.5, 173.4	173.7, 173.6
NCS	140.8	140.8	140.8	140.8	140.9	–	–	–
C-1	99.5	99.5	99.6	99.6	99.5	101.0	101.3	102.3
C-2	60.9	60.8	60.8	60.9	60.9	58.3	58.9	58.9
C-3	71.0	71.3	71.7	71.5	71.1	71.2	71.5	73.2
C-4	74.7	74.7	74.6	74.6	74.7	74.7	75.3	77.5
C-5	73.4	73.4	73.4	73.4	73.4	73.2	72.5	73.4
C-6	61.6	61.6	61.6	61.6	62.1	62.6	63.0	62.8
acyl-C	33.9, 31.3, 24.5 22.4, 13.9	34.0, 31.8, 29.5 24.9, 22.7, 14.1	34.0, 31.8, 29.4 24.9, 22.7, 14.1	34.1, 31.9, 29.4 24.9, 22.7, 14.1	– –	33.9, 31.3, 24.5 22.3, 13.9	34.0, 31.3, 24.5 22.3, 14.0	34.0, 31.3, 24.5 22.4, 13.9
Others	–	–	–	–	133.4, 129.4, 128.6 (benzoyl aromatic-C)	132.6, 129.9, 124.8 (phenyl aromatic-C)	46.8, 24.9, 11.4 (propyl-C)	49.2, 25.6, 22.5 (piperidyl-C)
FT-IR (cm^{-1})								
	2958, 2872, 2047 1747, 1462, 1379 1278, 1167, 1059 918, 777, 721	2926, 2855, 2043 1748, 1468, 1379 1279, 1159, 1059 916, 721	2924, 2853, 2047 1748, 1464, 1373 1278, 1165, 1062 920, 721	2924, 2853, 2043 1748, 1466, 1377 1278, 1163, 1061 922, 721	3062, 2029, 1728 1601, 1450, 1315 1269, 1093, 1066 935, 710	3347, 2957, 2870 1747, 1537, 1499 1377, 1356, 1242 1167, 1107, 1053 750, 696	3366, 2959, 2872 1748, 1547, 1456 1377, 1356, 1244 1168, 1110, 1053 754, 696	3399, 2934, 2856 1748, 1541, 1495 1377, 1358, 1240 1169, 1110, 1053 752

[a] The DS (degree of substitution) were determined by elementary analyses.

was collected by centrifugation (3000 × *g*, 15 min), and dissolved in a small amount of CH_2Cl_2. The resulting CH_2Cl_2 solution was then added to MeOH (200 mL) in a drop-wise manner to give a precipitate, which was collected by centrifugation (3000 × *g*, 15 min). This precipitation/dissolution process was repeated three times. The solid product was then dried in vacuo at 40 °C to afford compound **6** (29 mg).

Compound **6** – $DS_{TPPNHCS}$: 0.46 (determined by elemental analysis); FT-IR: *ν* 3415(NH), 2957, 2870, 2047, 1747 (C=O), 1537, 1498, 1377, 1356, 1242, 1167, 1107, 1053, 750, 696 cm^{-1}; ^1H NMR ($CDCl_3$): *δ* 8.80, 8.53, 8.18, 7.97, 7.73, 7.38 (porphyrin-H), 5.40–3.10 (H-1, H-2, H-3, H-4, H-5, H-6a, H-6b), 2.36 (hexanoyl $-OCOCH_2-$), 1.60 (hexanoyl $-OCOCH_2-CH_2-$), 1.26 (hexanoyl $-CH_2-$), 0.88 (hexanoyl $-CH_3$), −2.80 (NH of porphyrin) ppm.

2.4.2. Preparation and evaluation of LB monolayer films of compound 6

A solution of compound **6** in $CHCl_3$ (0.5 mg/mL) was spread onto a water subphase in a Teflon-coated trough (331 mm × 100 mm × 5 mm, USI-3-22T, USI-system, Fukuoka, Japan). Ultrapure water was obtained from a Milli-Q water purification system (Simpli Lab, Merck Japan, Tokyo, Japan) and used for the subphase. The solvent was evaporated for 30 min and the surface pressure (π)–area (A) isotherms were measured at a constant compression rate of 6 mm/min. The surface pressure was measured using a Wilhelmy-type film balance. The surface pressure was held at 10 mN m^{-1} for 30 min prior to the deposition of the surface monolayer onto the substrates. The vertical dipping method was used to deposit the surface monolayer onto the substrate with quartz, or an Indium Tin Oxide (ITO) electrode. The downward and upward stroke rates were set at 6 mm/min. The surface pressure was held at 10 mN m^{-1} throughout the deposition process, and the surface temperature was kept at 20 °C for the preparation of the LB monolayer films [i.e., film 6A (on quartz, transfer ratio: downward: 0.00, upward: 1.03), and film 6B (on an ITO electrode, transfer ratio: downward: 0.00, upward: 0.96)]. The photocurrent of film 6B was measured according to a previously reported method (Sakakibara et al., 2007).

3. Results and discussion

3.1. Preparation of acyl chitosan isothiocyanates

The *N*-phenylthiocarbamoylation of chitosan (**1**) was performed according to a slightly modified version of the method reported by Baba et al. (2002). It is noteworthy that the authors of this particular study only reported part of FT-IR data during their characterization of the structure of *N*-phenylthiocarbamoyl chitosan (**2**). In terms of the *N*-phenylthiocarbamoylation of chitosan (**1**), chitosan was reacted with phenyl isothiocyanate in a mixture of 5% (v/v) AcOH in water and MeOH at 35 °C for 24 h to afford compound **2** in 87.1% yield. The FT-IR spectrum of this compound (Supporting information 1) contained characteristic bands derived from phenylthiocarbamoyl groups at 1541, 1497, 746, and 692 cm^{-1} (Monier & Abdel-Latif, 2012; Shibano, Kamitakahara & Takano, 2013). ^1H and ^{13}C NMR analyses of compound **2** revealed signals around 7.0 and 125–135 ppm, which were assigned to the aromatic protons and carbons of the phenylthiocarbamoyl group, respectively. The ^{13}C NMR spectrum of compound **2** also contained a signal at 182.0 ppm, which was assigned to the C=S moiety of the phenylthiocarbamoyl group. The degree of substitution of the phenylthiocarbamoyl groups (DS_{PhNHCS}) in compound **2** was determined to be 0.86 by elemental analysis.

The hexanoylation of compound **2** was performed under typical acylation conditions (i.e., hexanoyl chloride and pyridine at

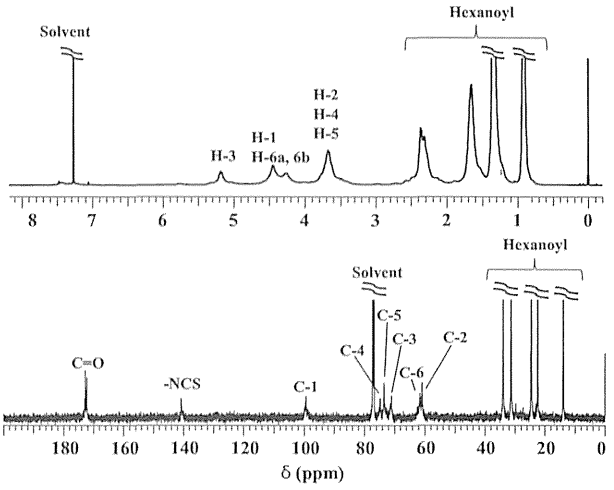

Figure 1. ^1H and ^{13}C NMR spectra of product A (compound **4a**).

0 °C for 1 h, 30 °C for 1 h, and 80 °C for 18 h sequentially) to give product A in high yield. Analysis of this compound by FT-IR revealed characteristic ester bands at 1747 and 1167 cm^{-1}, whereas the band around 3298 cm^{-1} corresponding to the hydroxyl groups and NH moieties of the thioureido groups of compound **2** were absent. Signals characteristic of the hexanoyl groups (Zong, Kimura, Takahashi & Yamane, 2000) were also found in the ^1H and ^{13}C NMR spectra of product A (Fig. 1). Taken together, these results suggested that hexanoylation had proceeded smoothly at both the *O*-3 and *O*-6 positions. In contrast, however, the characteristic bands of the phenylthiocarbamoyl groups at 1541, 1497, 746, and 692 cm^{-1} were not present in the FT-IR spectrum of product A. Furthermore, the aromatic signals of the phenyl moiety of the phenylthiocarbamoyl group around 7.0 and 125–135 ppm had disappeared from the ^1H and ^{13}C NMR spectra. These results therefore demonstrated, rather unexpectedly, that the phenylthiocarbamoyl groups were being removed from the chitosan during the hexanoylation process. The FT-IR spectrum of product A also contained a new band at 2047 cm^{-1}, which was consistent with the introduction of isothiocyanate (i.e., —NCS) groups (Shibano et al., 2013). Furthermore, this band disappeared when product A was reacted with an amine, which provided further evidence that this band related to the presence of NCS groups in product A. NMR analysis of provided further evidence in support of the presence of NCS groups in product A, with a signal consistent with the C=S moiety of the NCS group being observed at 140.8 ppm in the ^{13}C NMR spectrum (Fig. 1). Taken together, these data for product A indicated that this material was not 3,6-di-*O*-hexanoyl *N*-(hexanoyl)phenylthiocarbamoyl chitosan (**3a**) as expected, but 3,6-di-*O*-hexanoyl chitosan isothiocyanate (**4a**). The DS_{NCS} of compound **4a** was determined to be 0.74 by elemental analysis.

Fig. 2 shows the FT-IR spectra of the products resulting from the hexanoylation of compound **2** at various time points during the 80 °C heating stage of the reaction. The results of this analysis revealed that the characteristic bands of the ester and amide groups at 1747 and 1167 cm^{-1} and 1678 cm^{-1}, respectively, (Mohamed & Abd El-Ghany, 2012) appeared rapidly after only 1 h, whereas the bands attributed to the hydroxyl and thiourea groups at 3298 cm^{-1} were reduced significantly. These changes in the FT-IR spectra indicated that the *O*-hexanoylation of the 3-OH and 6-OH positions had proceeded smoothly, as well as the *N*-hexanoylation of the phenylthiocarbamoyl groups. The ^1H NMR spectrum of the product after 1 h, however, showed that the *O*-hexanoylation process

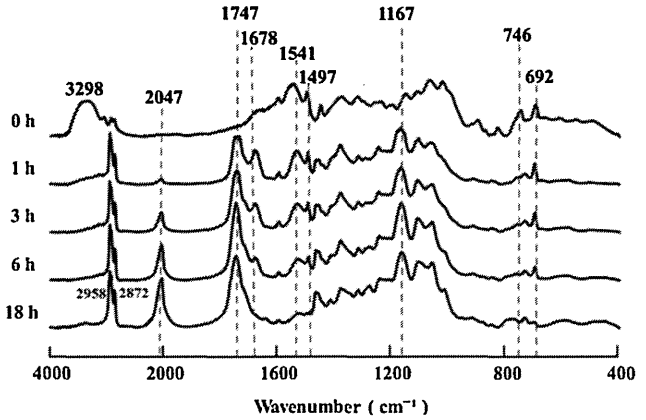

Figure 2. FT-IR spectra of the products during the 80 °C heating stage for the hexanoylation of compound **2** (normalized at 1379 cm^{-1}).

had not proceeded to completion (data not shown). The FT-IR spectrum of the product after 1 h of the 80 °C heating stage contained a small band at 2047 cm^{-1} for the NCS groups, which suggested that the *N*-phenylthiocarbamoyl groups were beginning to degrade during the first hour of this heating stage. As the reaction increased, there was an increase in the intensity of the band at 2047 cm^{-1}, whereas the intensities of the bands at 1678, 1541, 1497, 746, and 692 cm^{-1} decreased. After 18 h, the bands at 1678, 1541, 1497, 746, and 692 cm^{-1} were disappeared completely, suggesting that the *N*-(hexanoyl)phenylthiocarbamoyl groups had been fully degraded.

N,N′-Disubstituted thioureas are known to decompose to the corresponding amines and isothiocyanates when they are heated (Mukerjee & Ashare, 1991). For example, the pyrolysis of *N*-benzoyl-*N′*-phenylthiourea at 180 °C was reported to afford phenyl isothiocyanate in high yield (Rajappa, Rajagopalan, Sreenivasan & Kanal, 1979). Based on these reports and the FT-IR spectra shown in Fig. 2, we have proposed a mechanism for this transformation which is shown in Fig. 3. Briefly, the phenylthiocarbamoyl groups of compound **2** would be converted to the *N,N*-(hexanoyl)phenylthiocarbamoyl groups during *O*-hexanoylation process. The *N,N*-(hexanoyl)phenylthiocarbamoyl groups would then be degraded by the abstraction of a proton by pyridine, which would resulted in the formation of the NCS groups.

To evaluate the versatility of this method, we investigated the use of several other acylating agents for the acylation of

Table 2
Solubility of chitosan derivatives **2** and **4a–e**.

Solvents	δ	Compound					
		2	**4a**	**4b**	**4c**	**4d**	**4e**
THF	9.1	×	○	○	○	○	○
Chloroform	9.3	×	○	○	○	○	○
Acetone	9.4	×	○	△	△	×	○
Dichloromethane	9.6	×	○	○	○	○	○
Dioxane	9.8	×	○	○	△	△	○
DMF	11.5	○	○	△	△	×	○
DMSO	12.8	○	△	△	×	×	○
Methanol	12.9	×	×	×	×	×	×
Water	21.0	×	×	×	×	×	×

δ, Solubility parameter; ○, soluble; △, partially soluble; ×, insoluble.

compound **2** (i.e., dodecanoylation, myristoylation, stearoylation, and benzoylation) under the same conditions as those used for the hexanoylation reaction, which afforded compounds **4b–e** in high yields. The FT-IR spectra of compounds **4a–d** revealed that the characteristic bands of the phenylthiocarbamoyl groups at 1541, 1497, 746, and 694 cm^{-1} had disappeared, and that the characteristic bands of the NCS and ester groups had appeared around 2047 cm^{-1}, and around 1748 and 1159 cm^{-1}, respectively (Supporting information 1). These results indicated that the isothiocyanation reaction had proceeded in all cases regardless of the acyl group used in the acylation reaction. The DS_{NCS} values of compounds **4b–d** and **4e** were determined to be 0.70 and 0.56, respectively, by elemental analysis. The solubility of compound **2**, as well as those of compounds **4a–e** are summarized in Table 2. The acyl chitosan isothiocyanates **4a–e** were found to be soluble in a range of common solvents, including THF, $CHCl_3$, and CH_2Cl_2. Interestingly, however, compounds **4a–e** became insoluble in these solvents when they were stored as drying solids at ambient temperature for more than several days. Subsequent testing of the insoluble solid materials by FT-IR spectroscopy revealed that they were analytically identical to the initial solids (data not shown). Similar insolublization behavior has also been observed for compound **2** and 6-isothiocyanato cellulose derivatives (Shibano et al., 2013).

The *N*-phenylthiocarbamoylation of chitosan with phenyl isothiocyanate, followed by acylation with acyl chloride under basic conditions (i.e., in the presence of pyridine) has therefore been demonstrated as effective process for the preparation of acyl chitosan isothiocyanates. Furthermore, this method allows for the

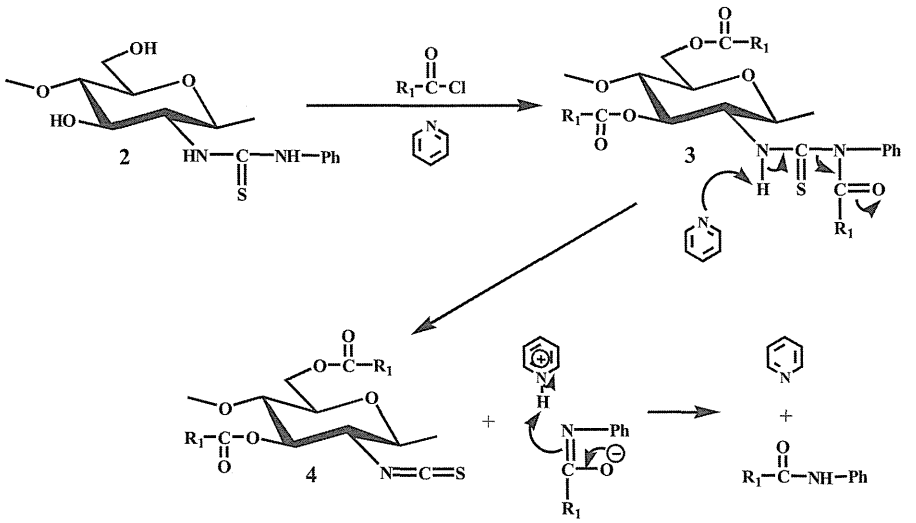

Figure 3. Proposed reaction mechanism for the formation of isothiocyanate groups.

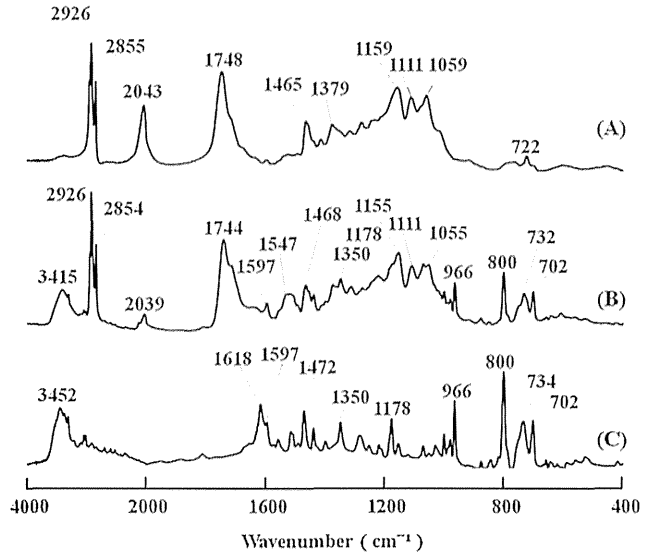

Figure 4. FT-IR spectra of compounds **4b** (A); **6** (B); and TPP-NH_2 (C).

use of harmful reagents such as thiophosgene to be avoided. In many ways, our newly developed method represents a trans-isothiocyanation reaction from a phenyl isothiocyanate to an acyl chitosan isothiocyanates in two reactions.

3.2. Reactivity of hexanoyl chitosan isothiocyanate *4a* with amines

Sugar isothiocyanates are known to react readily with amines to form thioureas (Pérez, Mellet, Fuentes & Fernández, 2000). To confirm it, we proceeded to investigate the reactivity of the acyl chitosan isothiocyanates toward a variety of amines. When compound **4a** was reacted with aniline (aromatic amine) in THF at 35 °C for 24 h, compound **5a** was formed in high yield. The FT-IR spectrum of compound **5a** contained the characteristic bands of the phenylthiocarbamoyl groups at 1537, 1497, 750, and 696 cm^{-1}, whereas the characteristic NCS band at 2047 cm^{-1} had disappeared. Furthermore, the ^{13}C NMR spectrum of compound **5a** contained a new signal at 181.0 ppm for the C=S moiety of the newly formed phenylthiocarbamoyl group, which indicated that the reaction of compound **4a** with aniline had proceeded smoothly. Compound **4a** was also reacted with propyl amine (aliphatic primary amine) and piperidine (aliphatic secondary amine) under the same conditions to give the corresponding compounds **5b** and **5c** in high yields, respectively. These results demonstrated that the acyl chitosan isothiocyanates were highly reactive toward amino compounds, and could therefore be used as intermediates for the synthesis of *N*-thiocarbamoyl chitosan derivatives.

3.3. Formation of a functional chitosan derivative from decanoyl chitosan isothiocyanate *4b*

The acyl chitosan isothiocyanate **4b** was converted to the porphyrin-appended chitosan derivative **6** to demonstrate the potential application of these compounds for the formation of functional chitosan derivatives. Compound **4b** was reacted with TPP-NH_2 in CH_2Cl_2 at 35 °C for 48 h to give compounds **6** in high yield. The FT-IR spectrum of compound **6** contained the characteristic bands of decanoyl chitosan at 2926, 2854, 1744, 1155, 1111, and 1055 cm^{-1}, as well as those from the porphyrin at 3415, 1597, 1468, 1350, 1178, 966, 800, 732, and 702 cm^{-1}, and those from the thiourea groups at 1547 cm^{-1} (Fig. 4). It is noteworthy that a small band corresponding to the NCS group was detected at 2039 cm^{-1}

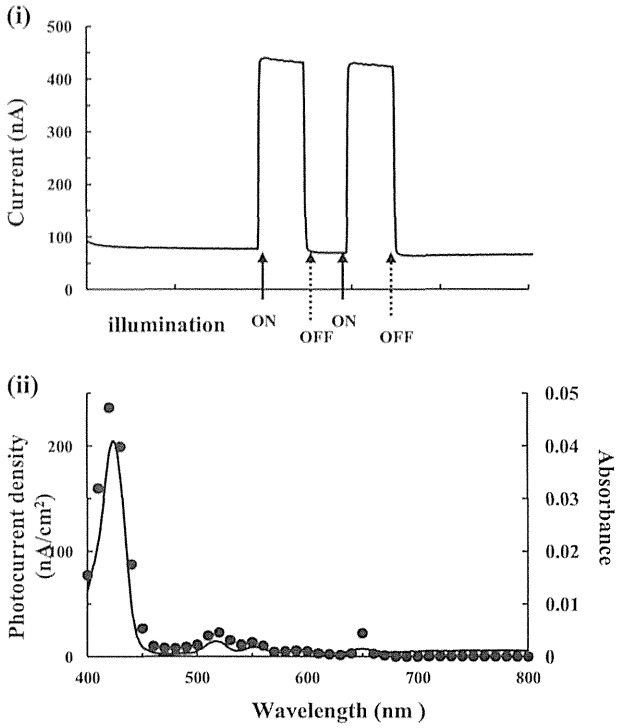

Figure 5. (i) Photoelectrochemical response of the LB monolayer film 6B with illumination at 420 nm; (ii) Action spectrum of film 6B (circles); UV–vis spectrum of film 6A (solid line).

in FT-IR spectrum of compound **6**, which indicated that the reaction with TPP-NH_2 had not proceeded to completion. The ^1H NMR spectrum of compound **6** contained signals from the aromatic protons of the porphyrin ring in the range 7.2–9.0 ppm, as well as the pyrrole-NH proton of the porphyrin ring at −2.80 ppm (Luguya et al., 2004) (Supporting information 2). The UV–vis spectrum of compound **6** in chloroform contained a Soret band in the range of 350–450 nm (Supporting information 3). These results clearly indicated that compound **6** was the expected porphyrin-appended chitosan derivative. The $DS_{TPPNHCS}$ value of compound **6** was determined to be 0.46 by elemental analysis. This medium DS value was attributed to the steric hindrance of the porphyrin groups, because a similar effect was also observed in the corresponding porphyrin-appended cellulose derivative (Sakakibara et al., 2007).

LB monolayer films of compound **6** were prepared on quartz (film 6A) and on an ITO electrode (film 6B) using the vertical dipping method with surface a pressure of 5 mN/m, which was decided based on the surface pressure (π)-area (A) isotherm of compound **6** at the air-water interface at 20 °C (Supporting information 4). In both cases, the monolayer film on the water was not transferred during the first down stroke, but was transferred during the second up stroke with a transfer ratio of almost 1.0, which indicated that films 6A and 6B were Z-type LB films. Film 6A was subjected to UV–vis analysis, whereas 6B was evaluated in terms of its photocurrent generation performance. The UV–vis spectrum of film 6A (solid state) had a similar profile to that of compound **6** in chloroform (solution state), which suggested that the monolayer had been successfully transferred. Fig. 5i shows the photoelectrochemical response of film 6B with illumination at 420 nm. The photocurrent was generated quickly when film 6B was illuminated. Fig. 5ii shows the action spectrum of film 6B (circles) and the UV–vis spectrum of film 6A (solid line). The patterns of these two spectra were very similar, which suggested that the porphyrin moieties of compound **6** were effectively behaving as photoactive species for the generation of the photocurrent, based on the absorption spectrum. The

photocurrent density (i.e., photocurrent per unit area of a working electrode) for film 6B at 420 nm was 236 μA/cm^2. This value was lower than that of an LB monolayer film constructed from a porphyrin-appended cellulose derivative, which had a $DS_{porphyrine}$ value of 0.64 (Sakakibara et al., 2007), and could therefore have been lower because of the lower DS_{TPPNH2} value of compound **6**. Taken together, these results suggest that compound **6** could be used as an effective alternative photon-to-electron conversion material in biomaterial-based solar cells.

4. Conclusion

A facile new method has been developed for the synthesis of for the preparation of acyl chitosan isothiocyanates based on the *N*-phenylthiocarbamoylation of chitosan followed by acylation of the resulting thiocarbamoylated material under basic conditions. Surprisingly, the formation of the NCS groups of the acyl chitosan isothiocyanates occurred as a consequence of the degradation of the *N,N*-(acyl)phenylthiocarbamoyl groups under the basic conditions required of the acylation reaction. A similar outcome was observed when the acylation reaction was conducted with acyl anhydride species under basic conditions, and the details of this alternative method will be published in our next paper.

The acyl chitosan isothiocyanates exhibited a high level of reactivity toward amines to afford the corresponding *N*-thiocarbamoyl chitosan derivatives, which suggested that various functional amines could be used to for the functionalization of chitosan. A porphyrin-appended chitosan derivative (**6**) was also prepared to evaluate the application of these acyl chitosan isothiocyanates to the synthesis of functional materials. The LB monolayer film of compound **6** gave a good photon-to-electron conversion performance, which suggested that compound **6** could be used as a promising photon-to-electron conversion material. Taken together, the results of this study demonstrate that our new method can be used to be provide rapid access to a range of acyl chitosan isothiocyanates, which have the potential to become useful intermediates for the construction of functional chitosan derivatives.

Acknowledgements

The authors thank to the funding program A-STEP FS stage Exploratory Research (FY2012) by Japan Science and Technology Agency.

Appendix A. Supplementary data

Supplementary data associated with this article can be found, in the online version, at http://dx.doi.org/10.1016/j.carbpol.2014.05.099.

References

Baba, Y., Noma, H., Nakayama, R., & Matsushita, Y. (2002). Preparation of chitosan derivatives containing methylthiocarbamoyl and phenylthiocarbamoyl groups and their selective adsorption of copper (II) and over iron (II). *Analytical Sciences, 18*, 359–361.

Fekry, A. M., & Mohamed, R. R. (2010). Acetyl thiourea chitosan as an eco-friendly inhibitor for mild steel in sulphuric acid medium. *Electrochimica Acta, 55*, 1933–1939.

Fernández, J. M. G., & Mellet, C. O. (1999). Chemistry and developments of *N*-thiocarbamoyl carbohydrate derivatives: Sugar isothiocyanates, thioamides, thioureas, thiocarbamates and their conjugates. In D. Horton (Ed.), *Advances in carbohydrate chemistry and biochemistry* (55) (pp. 36–1359). Sandiego: Academic Press.

Fernández-Bolaños, J. G., Zafra, E., López, O., Robina, I., & Fuentes, J. (1999). Stereoselective synthesis of imidazolidine, imidazoline and imidazole *C*- and *N*-psudonucleosides. *Tetrahedron: Asymmetry, 10*, 3011–3023.

Gaware, V. S., Håkerud, M., Leósson, K., Jónsdóttir, S., Høgset, A., Berg, K., et al. (2013). Tetraphenylporphyrin tethered chitosan based carried for photochemical transfection. *Journal of Medicinal Chemistry, 56*, 807–819.

Harish Prashanth, K. V., & Tharanathan, R. N. (2007). Chitin/chitosan: Modifications and their unlimited application potential – An overview. *Trends in Food Science & Technology, 18*, 117–131.

Huang, G., Guo, C.-C., & Tang, S.-S. (2007). Catalysis of cyclohexane oxidation with air using various chitosan-supported metallotetraphenylporphyrin complexes. *Journal of Molecular Catalysis A: Chemical, 261*, 125–130.

Jochims, J. C., & Seegler, A. (1965). Isocyanato- und isothiocyanato-derivate des D-glucosamins. *Tetrahedron, 21*, 2611–2616.

Kurita, K. (2006). Chitin and chitosan: Functional biopolymers from marine crustaceans. *Marine Biotechnology, 8*, 203–226.

Luguya, R., Jaquinod, L., Fronczek, F. R., Vicente, M. G. H., & Smith, K. M. (2004). Synthesis and reactions of meso-(p-nitrophenyl)porphyrins. *Tetrahedron, 60*, 2757–2763.

Ma, O., Lavertu, M., Sun, J., Nguyen, S., Buschmann, M. D., Winnik, F. M., et al. (2008). Precise derivatization of structurally distinct chitosans with rhodamine B isothiocyanate. *Carbohydrate Polymers, 72*, 616–624.

Mohamed, N. A., & Abd El-Ghany, N. A. (2012). Preparation and antimicrobial activity of some carboxymethyl chitosan acyl thiourea derivatives. *International Journal of Biological Macromolecules, 50*, 1280–1285.

Monier, M., & Abdel-Latif, D. A. (2012). Preparation of cross-linked magnetic chitosan-phenylthiourea resin for adsorption of Hg(II), Cd(II) and Zn(II) ions from aqueous solutions. *Journal of Hazardous Materials, 209–210*, 240–249.

Mouya, V. K., & Inamdar, N. N. (2008). Chiosan-modifications and applications: opportunities galore. *Reactive and Functional Polymers, 68*, 1031–1051.

Mukerjee, A. K., & Ashare, R. (1991). Isothiocyanates in the chemistry of heterocycles. *Chemical Reviews, 91*, 1–24.

Munch, H., Hansen, J. S., Pittelkow, M., Christensen, J. B., & Boas, U. (2008). A new efficient synthesis of isothiocyanates from amines using di-*tert*-butyl dicarbonate. *Tetrahedron Letters, 49*, 3117–3119.

Muzzarelli, C., Toshi, G., Francescangeli, O., & Muzzarelli, R. A. A. (2003). Alkaline chitosan solutions. *Carbohydrate Research, 338*, 2247–2255.

Muzzarelli, R. A. A., & Muzarelli, C. (2005). Chitosan chemistry: Relevance to the biomedical sciences. In T. Heinze (Ed.), *Advances in polymer science* (vol. 186) (pp. 151–209). Berlin: Springer Verlag.

Pérez, V. M. D., Mellet, C. O., Fuentes, J., & Fernández, J. M. G. (2000). Synthesis of glycosyl(thio)ureido sugars via carbodiimides and their conformational behavior in water. *Carbohydrate Research, 326*, 161–175.

Qaqish, R. B., & Amiji, M. M. (1999). Synthesis of a fluorescent chitosan derivative and its application for the study of chitosan-mucin interactions. *Carbohydrate Polymers, 38*, 99–107.

Rajappa, S., Rajagopalan, T. G., Sreenivasan, R., & Kanal, S. (1979). Isothiocyanate transposition through a retro-ene reaction: Pyrolysis of acylthioureas. *Journal of the Chemical Society. Perkin Transactions, 1*, 2001–2004.

Ravi Kumar, M. N. V., Muzzarelli, R. A. A., Muzzarelli, C., Sashiwa, H., & Domb, A. J. (2004). Chitosan chemistry and pharmaceutical perspectives. *Chemical Reviews, 104*, 6017–6084.

Rinaudo, M. (2006). Chitin and chitosan: Properties and applications. *Progress in Polymer Science, 31*, 603–632.

Sahoo, D., Sahoo, S., Mohanty, P., Sasmal, S., & Nayak, P. L. (2009). Chitosan: A new versatile bio-polymer for various applications. *Designed Monomers and Polymers, 12*, 377–404.

Sakakibara, K., Ogawa, Y., & Nakatsubo, F. (2007). First cellulose Langmuir–Blodgett films towards photocurrent generation systems. *Macromolecular Rapid Communications, 28*, 1270–1275.

Shibano, M., Kamitakahara, H., & Takano, T. (2013). Tandem Staudinger/aza-Wittig reaction of 6-azido-6-deoxycellulose. *Carbohydrate Research, 382*, 25–29.

Sun, C., Hu, B., Zhao, D., & Liu, Z. (2012). Covalently immobilized Mn(III)deuteroporphyrin on chitosan: An efficient and recyclable catalyst for aerobic oxidation of cyclohexane. *Journal of Applied Polymer Science, 125*, E79–E87.

Sun, N., Li, B., Shao, J., Mo, W., Hu, B., Shen, Z., et al. (2012). A general and facie one-pot process of isothiocyanates from amines under aqueous conditions. *Beilstein Journal of Organic Chemistry, 8*, 61–70.

Takano, T., & Shibano, M. (2013). Chitosan isothiocyanate derivative and method for producing same, WO201318767A1.

Zhong, Z., Xing, R., Liu, S., Wang, L., Cai, S., & Li, P. (2008). Synthesis of acyl thiourea derivatives of chitosan and their antimicrobial activities in vitro. *Carbohydrate Research, 343*, 566–570.

Zong, Z., Kimura, Y., Takahashi, M., & Yamane, H. (2000). Characterization of chemical and solid state structures of acylated chitosans. *Polymer, 41*, 899–906.

DOI 10.1515/hf-2013-0164 — Holzforschung 2014; 68(7): 747–760

Yasuyuki Miyagawa*, Takahito Mizukami, Hiroshi Kamitakahara and Toshiyuki Takano

Synthesis and fundamental HSQC NMR data of monolignol β-glycosides, dihydromonolignol β-glycosides and *p*-hydroxybenzaldehyde derivative β-glycosides for the analysis of phenyl glycoside type lignin-carbohydrate complexes (LCCs)

Abstract: Twelve monolignol (coniferyl alcohol, sinapyl alcohol and *p*-coumaryl alcohol) β-glycosides (β-glucosides, β-galactosides, β-xylosides and β-mannosides) were synthesised to obtain fundamental NMR data for the analysis of phenyl glycoside type lignin-carbohydrate complexes (LCCs). That is, the 1,2-*trans* glycosides (the β-glucosides, β-galactosides and β-xylosides) and the 1,2-*cis* glycosides (the β-mannosides) were synthesized by means of Koenig-Knorr glycosylation and β-selective Mitsunobu glycosylation strategies, respectively. In addition, dihydromonolignol and *p*-hydroxybenzaldehyde derivative β-glycosides were also prepared from the corresponding monolignol glycosides and their intermediates, respectively. The correlation observed for the $C_{1\beta}$-$H_{1\beta}$ bonds of the sugar moieties in the HSQC spectra of the all β-glycosides varied and were in the range of δ_C/δ_H 96–104/4.7–5.4 ppm. Especially, it was found that the correlations derived from the $C_{1\beta}$-$H_{1\beta}$ bonds of the guaiacyl and *p*-hydroxyphenyl β-mannosides were close to those derived from the $C_{1\alpha}$-$H_{1\alpha}$ bonds of the 4-*O*-methyl-α-D-glucuronic acid moieties described in the literature.

Keywords: catalytic hydrogenation, ^{13}C NMR, deisopropylidenation, HSQC NMR, Knoevenagel condensation, Koenig-Knorr glycosylation, lignin-carbohydrate complex (LCC), β-mannoside, Mitsunobu glycosylation, monolignol β-glycoside, phenyl glycoside, reduction with DIBAL-H, synthesis of lignin model compounds

***Corresponding author: Yasuyuki Miyagawa,** Division of Forest and Biomaterials Science, Graduate School of Agriculture, Kyoto University, Kyoto, Japan, e-mail: takatmys@kais.kyoto-u.ac.jp
Takahito Mizukami, Hiroshi Kamitakahara and Toshiyuki Takano: Division of Forest and Biomaterials Science, Graduate School of Agriculture, Kyoto University, Kyoto, Japan

Introduction

Lignin carbohydrate complexes (LCCs) can cause problems during pulping and biorefining processes, because they aggravate the selective separation of the essential wood components (Henriksson et al. 2007; Balakshin et al. 2008; Li et al. 2011). The main lignin-carbohydrate (LC) linkages present in LCCs have been reported to be α-ethers, γ-esters and phenyl glycosides (Koshijima and Watanabe 2003; Balakshin et al. 2008). However, the structural elucidation of the LC linkages in LCCs remains challenging (Balakshin et al. 2007; Westbye et al. 2008; Ando et al. 2012, 2013; Miyagawa et al. 2012). Especially, the reports pertaining to phenyl glycoside type LC linkage as well as the biosynthetic processes involved in their construction are scarce in the literature, although the linkages are supposed to form between phenolic hydroxyl groups of lignin moieties and C-1 hydroxyl groups at the reducing-end of polysaccharides (Fengel and Wegener 1983; Lai 2001).

2D NMR methods, including heteronuclear single-quantum coherence (HSQC) in particular, have recently become powerful tools for the analysis of lignin structures (Ralph et al. 1999; Kim et al. 2008; Rencoret et al. 2009; Kim and Ralph 2010; Mansfield et al. 2012), and the identification of different LC linkages. With regard to the HSQC analysis of phenyl glycoside type LC linkages, Balakshin et al. (2011) reported several correlations in the 2D HSQC spectra of crude milled wood lignin (MWL) and the acetic acid extracts of pine and birch in the range of δ_C/δ_H 99–104/4.8–5.2 ppm. These correlations were reported to be derived from the C_1-H_1 bonds of the sugar moieties of the phenyl glycosides type LC linkages, with some of the these signals occurring as a consequence of LC linkages to different types of carbohydrates. Yuan et al. (2011a) reported the occurrence of several correlations in the 2D HSQC spectra of MWL and the lignin